RM A57A24

NACA RM A57A24

NACA

RESEARCH MEMORANDUM

WIND-TUNNEL TESTS OF THE STATIC LONGITUDINAL CHARACTERISTICS AT LOW SPEED OF A SWEPT-WING AIRPLANE WITH SLOTTED FLAPS, AREA-SUCTION FLAPS, AND WING LEADING-EDGE DEVICES

By Ralph L. Maki and Harry A. James

Ames Aeronautical Laboratory
Moffett Field, Calif.

NATIONAL ADVISORY COMMITTEE
FOR AERONAUTICS

WASHINGTON

April 30, 1957

NATIONAL ADVISORY COMMITTEE FOR AERONAUTICS

RESEARCH MEMORANDUM

WIND-TUNNEL TESTS OF THE STATIC LONGITUDINAL CHARACTERISTICS AT LOW SPEED OF A SWEPT-WING AIRPLANE WITH SLOTTED FLAPS, AREA-SUCTION FLAPS, AND WING LEADING-EDGE DEVICES

By Ralph L. Maki and Harry A. James

SUMMARY

A low-speed wind-tunnel investigation of a high-wing airplane with an aspect ratio of 6.75 and 36° sweepback of the quarter-chord line was conducted to determine the lift increments obtainable with area-suction flaps. Comparisons were made with the characteristics of the airplane with the slotted flaps normally used. The flaps were tested in conjunction with various combinations of leading-edge devices to increase maximum lift and to maintain longitudinal stability throughout the lift range.

Flap lift increments were approximately equal to those predicted by theory in the low lift-coefficient range. Lift at high angles of attack was limited by flow separation at the wing leading edge. Inboard high-lift devices at the wing leading edge were effective in increasing maximum lift. The relative lift effectiveness of inboard and outboard leading-edge devices determined the longitudinal stability characteristics. With area-suction flaps deflected 55°, installation of a simulated inboard nose flap and an increase in deflection of the outboard slat (from 17° to 24°) increased the maximum lift coefficient from about 1.6 without the devices to about 2.2, and delayed the onset of noticeable airplane buffeting from an angle of attack of about 5° to about 12°.

Critical flow coefficients of about 0.0006 with 55° deflection and 0.0004 with 45° deflection were measured for the area-suction flaps with a porous surface having constant porosity.

No significant changes in the low-speed characteristics resulted when the sweep of the inboard portion of the flap hinge line was reduced by increasing the wing root chord length.

INTRODUCTION

The general boundary-layer-control research program at the Ames Aeronautical Laboratory has included investigations of the effectiveness of area-suction flaps on wings with a wide range of plan forms. Common to all these studies is the attainment of sizable incremental lift coefficients at low angles of attack due to area-suction applied to deflected trailing-edge flaps. For wings with angles of sweepback of about 35° and larger, these gains in lift coefficient are often reduced and even lost at moderate angles of attack due to flow separation initiating at the wing leading edge (e.g., ref. 1). When this flow separation originates over the outboard portions of the swept wing panels, serious losses in longitudinal stability accompany the decreases in flap lift increment. It has been shown that the leading-edge flow separation can be delayed by suitable high-lift devices at the wing leading edge, and that the changes in longitudinal stability can be controlled by proper spanwise extents of these leading-edge devices.

As part of the general boundary-layer-control program, a study has been made in the Ames 40- by 80-foot wind tunnel of the application of area-suction trailing-edge flaps to an airplane with a high aspect ratio (6.75) wing plan form and moderate sweepback (35.9°), complicated by outboard engine nacelles subtended on pylons at the 39-percent semispan stations. The wing plan form was altered for parts of the program by increasing the root chord length and unsweeping the inboard portion of the trailing-edge flaps. Besides the assessment of flap lift effectiveness, it was desired to attain increases in maximum lift while preserving satisfactory static longitudinal stability by controlling the spanwise stall progression by means of wing leading-edge high-lift devices, as discussed above.

Tests were made of the basic airplane equipped with slotted flaps to provide directly comparable data for evaluation of the area suction plain flap results. The discussion is limited to an analysis of results which relate to the problems stated above. The balance of the test data is presented without discussion. Results of tests with wing fences and of control effectiveness are included.

NOTATION

All force and moment coefficients are based on the original wing area of the test airplane. Pitching moments are referred to an axis joining the quarter-chord points of the mean aerodynamic chords of the wing panels.

A	aspect ratio
b	span
c	wing chord, measured streamwise
$\bar{c}$	mean aerodynamic chord, $\dfrac{\int_0^{b/2} c^2 dy}{\int_0^{b/2} c\, dy}$
C_D	drag coefficient
C_L	lift coefficient
C_l	rolling-moment coefficient
C_m	pitching-moment coefficient
C_n	yawing-moment coefficient
C_p	pressure coefficient, $\dfrac{p_l - p_\infty}{q_\infty}$
C_Q	suction-air flow coefficient, $\dfrac{Q}{VS}$
C_Y	side-force coefficient
p_d	suction-duct static pressure
p_l	local static pressure
p_∞	free-stream static pressure
Q	suction-air volume rate of flow, corrected to sea-level standard conditions
q_∞	free-stream dynamic pressure
R	Reynolds number, $\dfrac{V\bar{c}}{\nu}$
S	original wing area of test airplane
V	free-stream velocity
x	streamwise distance from unmodified wing leading edge with slat closed
x_n	distance from unmodified wing leading edge with slat closed measured normal to leading edge

y spanwise distance, measured normal to fuselage center line

y_s spanwise distance, measured along 0.15 chord line

y_f spanwise distance, measured along 0.77 chord line

z height above wing chord plane

α airplane angle of attack, measured with respect to the fuselage center line

α_δ flap lift-effectiveness parameter, $\frac{dC_L/d\delta_f}{dC_L/d\alpha}$

ΔC_L flap lift increment, measured at constant angle of attack

δ_f trailing-edge-flap deflection, measured normal to hinge line

η fraction of semispan, $\frac{y}{b/2}$

ν kinematic viscosity

Subscripts

crit critical

L left

max maximum

R right

T due to wind-tunnel-wall interference

W wing

MODEL AND APPARATUS

General Model Information

The test airplane had a high wing of aspect ratio 6.75 and 35.9° sweepback of the quarter-chord line in the wing reference plane. This wing will be referred to as plan form 1. Note that model angle of attack is referred to the fuselage reference line, and the wing is attached at

an incidence of 4°. Engine nacelles are subtended below and forward of the wing panels on pylons at 0.39 semispan. Pertinent geometric details are listed in table I and a sketch is presented as figure 1.

Figure 2 is a photograph of the model mounted in the test section of the wind tunnel. The strut support mounts were attached at the main wheel axles and arrestor-hook pivot point. The bomb-bay doors, nose-wheel door, speed brakes, and tail bumper wheel remained closed for all tests. The vertical fin was removed at the fold line. The engines were removed, and air was allowed to flow freely through the nacelles. The wing slats were locked in either the closed or open positions.

Alternate Plan Form

The wing plan form was modified over the inboard region near the trailing edge for some of the tests. This alternate wing plan form is designated herein as plan form 2. The principal change is an increase in root chord reducing the sweep of a portion of the flap hinge line. The location of this root fillet, triangular in shape, is described in figure 1 and shown in the photograph of figure 3. The root section incorporated camber near the trailing edge (see fig. 4). The camber was diminished by straight-line-element fairing to meet the uncambered section of plan form 1 at the flap juncture line. No attempt was made to form any prescribed airfoil thickness distribution in the fillet region, since this would have required wing thickness changes extending well forward of the suction-flap hinge line on plan form 1. The upper surface was faired smoothly, and unavoidable surface slope discontinuities were restricted to the lower surface.

Wing Trailing-Edge Flaps

The basic airplane was equipped with 0.25 c slotted flaps. Maximum flap deflection was 36°.

The boundary-layer control flaps were 0.23 c plain flaps with provisions for applying boundary-layer control by suction at the knee of the flaps as shown in figure 4. Deflections of 45° and 55° were provided on plan form 1, and deflections of 0° and 55° on plan form 2. Because of the difference in hinge-line sweep angle on the inboard and outboard sections of the flap on plan form 2, the trailing edge at the juncture line was discontinuous with flaps deflected. This gap was unsealed for most tests. The porous area for the suction-flap installations was formed with a metal-mesh surface sheet (4225 holes per square inch) backed by felt cloth. The extent of the porous surface is described in figure 4. The porosity was constant in both chordwise and spanwise directions. The

flow characteristics are given in figure 5. The wing region between the rear spar and the flap was sealed to serve as a duct for the boundary-layer air.

Boundary-Layer Control System

An aircraft-type supercharger compressor driven by two 300-horsepower electric motors was installed in the bomb bay of the test airplane as a power unit for boundary-layer air removal. Collectors at the fuselage walls at the root of the wing ducts delivered the boundary-layer air from the flap duct region into flexible lines which led to a plenum chamber attached to a supercharger. The flow was measured with a thin-plate orifice in a pipe attached to the blower exit. Boundary-layer air was discharged through the partially open cockpit escape hatch which was located on the lower surface of the fuselage forward of the bomb bay. Maximum flow quantity of the system was about 130 cubic feet per second at the duct pressures encountered during the tests.

Wing Leading-Edge Devices

Two full-span leading-edge gloves incorporating forward camber and enlarged leading-edge radii were tested. Coordinates for these gloves are given in table II. Camber and leading-edge radii for glove 2 are larger than for glove 1. Glove 2 also was installed as a partial-span device for some tests, extending only from the wing root to the nacelle pylons, in which cases it is called glove 2i. Glove 3i which was similar to glove 2i was used on tests of plan form 1 with slotted flaps.

The glove 2 profiles were adapted to the normal slats in their extended position for some tests. These modified contours were positioned such that the resulting deflection was 24° as compared to 17° deflection of the normal slat. Example profiles are shown in figure 6. The spanwise extent of the modification was varied, allowing the effect of extents of this modification designated as M_1, M_2, M_3, and M_4 to be measured (see fig. 1): in all cases the entire span of the normal slat was extended.

Glove 4i was highly cambered to simulate a deflected nose flap. It extended from the wing root to the nacelle pylons. A typical profile of this device is shown in figure 7; coordinates are included in table II.

Other Test Devices

Full-chord upper-surface wing fences were installed on plan form 1 at 0.39, 0.62, and 0.85 b/2. The fences at 0.62 and 0.85 b/2 were 5-percent chord high with a leading-edge wrap-around to 5-percent chord on the lower surface (see fig. 7). The fence at 0.39 b/2 terminated flush with the pylon leading edge.

A revised pylon leading edge was installed for most of the tests which extended the pylon leading edge forward and faired into the wing upper surface at 5-percent chord. The cross-section contour near the leading edge was kept approximately the same as the original pylon. The modified pylon is sketched in figure 7.

TESTS AND CORRECTIONS

The majority of the tests were made at a dynamic pressure of about 15 pounds per square foot. This corresponds to a Reynolds number of about 8.2×10^6 based on the wing mean aerodynamic chord. A few configurations were also tested at Reynolds numbers of about 10.5 and 13.4×10^6 to span the current approach-speed range for this type of airplane. Because of excessive airplane buffeting at high angles of attack, only a brief study was made at these higher tunnel speeds.

The test airplane was unusually large relative to the tunnel test-section dimensions. The wing-span to tunnel-width ratio was 0.91. Theoretically determined interference effects of the wind-tunnel walls are therefore of doubtful accuracy, but were nevertheless applied to the data. The wall-interference corrections added were as follows:

$$\alpha_T = 1.40\ C_L$$

$$C_{D_T} = 0.024\ C_L^2$$

$$C_{m_T} = 0.039 \text{ (tail-on data only)}$$

The data have been corrected for stream-angle inclinations. The effects of the tunnel support struts, of removing the vertical fin above the fold line, of the strut mounting blocks on the main wheel axles, and of the partially open cockpit access door (boundary-layer configurations only) are unknown.

RESULTS

In the discussion to follow, selected test results which relate to evaluation of flap lift effectiveness, improvements in $C_{L_{max}}$, maintenance of longitudinal stability, and suction requirements are treated. These results are presented in figures 8 to 14. The complete force data recorded in the investigation, together with suction air-flow data and limited flap pressure data, are presented in figures 15 to 32.

Unless otherwise designated on a figure, it shall be assumed that the test configuration includes the following:

1. Slats locked closed.
2. Horizontal-tail incidence setting of -4°.
3. Elevators locked at 0° and ailerons at $1\text{-}1/2^{\circ}$ trim setting (trailing edge up).
4. Modified pylon leading edges.
5. Engine nacelles open.
6. $C_Q = 0.001$ for tests with area-suction flaps deflected with boundary-layer control operating.
7. No auxiliary devices (e.g., fences or tufts).

DISCUSSION

As the test program progressed, it became apparent that the control of air-flow separation at the wing leading edge was of primary importance when a high-lift flap was employed. It was demonstrated that both maximum lift and longitudinal stability became increasingly dependent on the leading-edge configuration as the flap lift was increased. This point will be examined by considering selected results from tests of the airplane with slotted flaps (plan form 1) and with area-suction flaps on plan form 2. The latter plan form was chosen over plan form 1 for the discussion of area-suction-flap results because a more complete sequence of data was taken. Comparison of incremental differences from tests of otherwise identical conditions for plan forms 1 and 2 show that only small differences exist.

Flap Lift

The flap lift increments measured at low angles of attack are compared with theoretical values in the following table.

Type of flap	δ_f, deg	ΔC_L due to flaps	
		Theoretical	Measured
Slotted	36	0.74	0.75 (from fig. 8)
Area suction	55	1.11	1.06 (from fig. 12)

The measured flap lift increments varied somewhat with wing leading-edge configuration, being as much as 10 percent lower in one case with suction flaps deflected 55°. The theoretical values were computed by the theory of reference 2 using the geometry of plan form 1 in both cases and α_δ values from the curve labeled "theory" in figure 3 of reference 2. From the comparisons, it can be concluded that, where no separation from the wing leading edge existed, the flaps gave approximately the lift increments to be expected.

Maximum Lift and Stability

Basic wing.- Shown in figure 8 are the characteristics of the basic wing with slotted flaps at 0° and 36° deflection, and slats both open and closed. The drag and pitching-moment variations above an angle of about 9° with slats closed and flaps up are typical of those due to flow separation originating at the tips of swept wings and spreading inboard with increase in angle of attack. In this case the variations occurred some 8° before maximum lift. With slats open (flaps undeflected) the lift and pitching-moment curves were linear to higher angles of attack, indicating that the outboard slats protected the tip region; however, drag data and tuft observations showed that flow separation started from the unprotected leading edge between the pylons and fuselage at about 13° angle of attack. While the lift and pitching-moment variations were substantially improved by extending the slats, the drag level was high and roughness (as evidenced by visible airplane buffeting) appeared at high lifts. It will be noted that the results being discussed concern configurations with the horizontal tail on. Directly comparable data for two wing configurations with the horizontal tail off and on are given in figures 17 and 20, respectively. These data show the tail has a generally stabilizing influence on the pitching-moment changes at high lift.

Deflecting the flaps with the slats closed caused the wing tips to stall at about 6° angle of attack (fig. 8). The stall spread inboard so quickly with increasing α that extreme instability and rapid loss of flap lift increment resulted. Extension of the slats with the flaps

deflected controlled the tip stall and virtually eliminated the instability, an effect similar to that with flaps undeflected. However, flow separation again appeared inboard of the pylons only 3° later than the tip region had stalled with slats closed. As α was further increased, the drag level was high and the flow rough, similar to the slats-open, flaps-undeflected case.

Glove 3i was installed between the pylons and fuselage in an attempt to suppress the leading-edge stall in this region. It delayed the inboard stall with flaps either up or down (about 5° according to tuft observations), but did not materially change the lift characteristics at high angles of attack.

Plan form 2 with area-suction flaps deflected 55°.- Installation of the area-suction flaps, while retaining the basic wing leading edge with slats open, resulted in the appearance of leading-edge flow separation inboard of the pylons about 6° angle of attack earlier than with the slotted flaps at 36° deflection. This can be discerned in the drag and pitching-moment data in figures 8 and 10. Loss of wing lift due to this leading-edge flow separation rapidly reduced the lift increment provided by the boundary-layer control effect, so that a few degrees above the onset of separation the lift was no greater than for the flap deflected without boundary-layer control, and considerably less than with the slotted flaps deflected. It was apparent that the higher loading induced inboard by the area-suction flaps caused this region of the wing to stall long before the outboard regions had reached their maximum lift.

In an effort to delay the inboard flow separation, the wing leading edge from fuselage to pylons was modified by installing glove 4i which resulted in a contour comparable to a nose flap deflected about 30° (described in fig. 7). It can be seen from the results presented in figure 11 that this leading-edge device had a powerful effect on the stall characteristics, delaying the inboard stall for about 6° angle of attack with boundary-layer control operative. As a result, a useful flap lift increment due to boundary-layer control was maintained to $C_{L_{max}}$, and $C_{L_{max}}$ was increased from about 1.6 to 2.15.

With the above configuration, tuft observations indicated incipient separation in the wing tip region near $C_{L_{max}}$ and, hence, instability might be imminent. The wing slats were therefore modified as shown in figure 6 to increase their effectiveness as a leading-edge device. The modification was installed in two steps, first from the wing tips to a point corresponding approximately to the span position of the outboard end of the trailing-edge flap (M_2), and then over the entire slat span (M_3). The test results are given in figure 12. Modification M_2 had little effect beyond increasing the nose-down moment after $C_{L_{max}}$. Modification M_3 resulted in an increase of lift-curve slope and a slight increase in $C_{L_{max}}$ to about 2.25. It is possible that further improvement

of the leading-edge devices would provide additional gains in $C_{L_{max}}$. For example, if boundary-layer control methods were applied to leading-edge flaps, and the relative lift effectiveness of inboard and outboard devices again properly adjusted, further increases in $C_{L_{max}}$ would be anticipated.

A number of combinations of other leading-edge devices were tried, each indicating generally the same result, namely that a weakening of the leading-edge protection inboard reduced $C_{L_{max}}$, and a weakening outboard caused a tendency toward longitudinal instability. The test results presented in figures 16 to 26 include such configurations.

Boundary-Layer Control Requirements

No attempt was made to minimize the boundary-layer air-flow requirements in these tests in which material of constant porosity was used. The study reported in reference 3 showed reductions of as much as 55 percent in critical flow coefficient by selection of proper magnitude and variation of chordwise pressure drop across the porous area. The tests with all suction flaps on plan form 2 and most suction flaps on plan form 1 were made with a constant chordwise length of opening of porous area from 1/2 inch forward to 3 inches behind the mid-arc reference line (see fig. 4). The forward edge of the opening was very nearly at the position of minimum surface pressure, as recommended in reference 3 as one requirement for minimizing the required suction flow quantity. The constant chordwise length of opening was chosen in order to have a relatively greater quantity of boundary-layer air withdrawn near the flap tips. Typical variations of lift due to suction with flow coefficient C_Q are shown in figure 13. Example surface pressure distributions over the porous area and suction duct pressures are shown in figure 14. The methods outlined in reference 3 were applied to estimate critical values of C_Q and duct pressures. The estimated values are compared with the measured values in the table below. Data at 45° deflection are those recorded for tests with plan form 1.

δ_f, deg	$C_{Q_{crit}}$		Average duct pressure ratio at $C_{Q_{crit}}$	
	Estimated	Measured	Estimated	Measured
45	0.00038	0.0004	1.023	1.02 (data of fig. 25)
55	.00068	.0006	1.032	1.03 (data of fig. 14)

The estimated values agree quite closely with the measured results for both 45° and 55° area-suction flaps.

The duct pressure ratios are referenced to the wind-tunnel test speed which was quite low as compared with the approach speed range of the

airplane. If the measured values at 55° flap deflection were applied to an airplane with a wing loading of 64.1 pounds per square foot (50,000 pounds weight), and a pumping system designed to provide $C_{Q_{crit}}$ (0.0006) at a conservative approach speed of 120 knots ($1.3V_{stall}$), the required pressure ratio would be 1.115. As speed is reduced in the approach, the available C_Q would, of course, increase whereas $C_{Q_{crit}}$ stays essentially constant. At V_{stall} the system would provide a C_Q of about 0.00078.

CONCLUDING REMARKS

A low-speed wind-tunnel investigation was conducted on a high-wing airplane of aspect ratio 6.75 and 36° sweepback fitted both with slotted flaps and with area-suction plain flaps. An alternate wing plan form with an extended root chord and lesser sweepback of the inboard portion of the flaps was also tested with area-suction plain flaps.

Flap lift increments at low angles of attack were approximately equal to those predicted by theory.

Flap lift increments at high angles of attack were reduced by stall at the wing leading edge. High-lift devices extending from the fuselage to the nacelle pylons (at 0.39 semispan) were effective in maintaining flap lift increments at high angles of attack and in increasing maximum lift. Longitudinal stability depended on the lift effectiveness of devices outboard of the pylons. The addition of a simulated inboard nose flap and an increase in deflection of the outboard slat (from 17° to 24°) increased maximum lift with area-suction flaps deflected 55° on the alternate plan form from about 1.6 to about 2.2. The onset of noticeable airplane buffeting was delayed from an angle of attack of about 5° for the basic airplane to about 12°.

Critical flow coefficients of about 0.0006 and 0.0004 were measured for area-suction flaps at 55° and 45° deflection, respectively, with a porous surface having constant porosity.

No significant differences were found in the results with the two wing plan forms tested.

Ames Aeronautical Laboratory
National Advisory Committee for Aeronautics
Moffett Field, Calif., Jan. 24, 1957

REFERENCES

1. Griffin, Roy N., and Hickey, David H.: Investigation of the Use of Area Suction to Increase the Effectiveness of Trailing-Edge Flaps of Various Spans on a Wing of 45° Sweepback and Aspect Ratio 6. NACA RM A56B27, 1956.

2. DeYoung, John: Theoretical Symmetric Span Loading Due to Flap Deflection for Wings of Arbitrary Plan Form at Subsonic Speeds. NACA Rep. 1071, 1952.

3. Cook, Woodrow L., Holzhauser, Curt A., and Kelly, Mark W.: The Use of Area Suction for the Purpose of Improving Trailing-Edge Flap Effectiveness on a 35° Sweptback Wing. NACA RM A53E06, 1953.

TABLE I.- GEOMETRIC DATA ON THE TEST AIRPLANE

Wing	
Area, sq ft (plan form 1)	780.0
Area added by fillet on plan form 2, sq ft	29.7
Span, ft	72.50
Aspect ratio	6.75
Taper ratio	0.34
Mean aerodynamic chord, ft	11.68
Sweepback of the quarter-chord line, deg	35.9
Incidence, deg	4
Dihedral, deg	0
Twist, deg	0
Root airfoil (streamwise, fuselage center line)	NACA 63-009.95 (mod.)
Tip airfoil (streamwise, b/2 = 435 in.)	NACA 63-008.25 (mod.)
Span of one flap, ft	16.84
Inboard end of flap, feet from fuselage center line	4.00
Flap chord, percent of wing chord (slotted flap)	25
Span of one slat, ft	21.42
Inboard end of slat, feet from fuselage center line	14.14
Slat chord at inboard end, percent wing chord	16.9
Slat chord at wing tip, percent wing chord	24.3
Slat deflection, deg	17
Horizontal Tail	
Area, sq ft	166.6
Span, ft	25.83
Aspect ratio	4.0
Taper ratio	0.50
Mean aerodynamic chord	6.75
Sweepback of the quarter-chord line, deg	33.9
Volume, $\frac{\text{tail length}}{\text{wing } \bar{c}} \times \frac{\text{tail area}}{\text{wing area}}$	0.53
Dihedral, deg	10
Height of tail above wing plane, ft	6.68
Elevator hinge location, percent tail chord	75
Fuselage	
Length, ft	71.19
Frontal area (excluding canopy), sq ft	50.4
Maximum width, ft	7.17

TABLE II.- COORDINATES OF THE LEADING-EDGE GLOVES, NORMAL TO THE WING LEADING EDGE

[Dimensions given in inches]

Glove 1					
Leading-edge station 71.00			Leading-edge station 539.00		
x_n	z_{upper}	z_{lower}	x_n	z_{upper}	z_{lower}
-4.30	-3.06	-3.06	-4.30	-2.23	-2.23
-4.11	-2.25	-3.82	-4.21	-1.94	-2.50
-3.92	-1.88	-4.10	-4.13	-1.79	-2.58
-3.54	-1.39	-4.45	-3.95	-1.57	-2.68
-3.16	-1.00	-4.69	-3.78	-1.41	-2.75
-2.79	-.65	-4.87	-3.61	-1.26	-2.79
-2.40	-.33	-5.03	-3.43	-1.13	-2.82
-.51	1.02	-5.54	-2.56	-.55	-2.91
3.31	3.02	-6.11	-.83	.30	-2.93
7.15	4.36	-6.50	.93	.93	-2.86
11.03	5.43	-6.83	2.70	1.42	-2.81
14.93	6.13	-7.14	4.48	1.81	-2.75
18.85	6.79	-7.43	6.27	2.12	-2.70
22.81	7.37	-7.71	8.07	2.37	-2.69
26.79	7.85	-8.00	9.89	2.57	-2.71
30.81	8.25	-8.28	11.72	2.73	-2.77
Glove 2					
-4.77	-3.96	-3.96	-4.77	-3.00	-3.00
-4.69	-3.34	-4.50	-4.69	-2.60	-3.73
-4.61	-3.07	-4.72	-4.61	-2.42	-3.50
-4.50	-2.78	-4.96	-4.49	-2.21	-3.62
-4.30	-2.40	-5.24	-4.30	-1.94	-3.75
-4.11	-2.10	-5.44	-4.21	-1.84	-3.79
-3.92	-1.83	-5.61	-4.13	-1.74	-3.82
-3.54	-1.39	-5.86	-3.95	-1.56	-3.88
-3.16	-1.00	-6.06	-3.78	-1.41	-3.92
-2.79	-.65	-6.21	-3.61	-1.26	-3.95
-2.40	-.33	-6.35	-3.43	-1.13	-3.97
-.51	1.02	-6.78	-2.56	-.55	-3.99
3.31	3.02	-7.10	-.83	.30	-3.81
7.15	4.36	-7.21	.93	.93	-3.60
11.03	5.34	-7.28	2.70	1.42	-3.31
14.93	6.13	-7.38	4.48	1.81	-3.05
18.85	6.79	-7.54	6.27	2.12	-2.85
22.81	7.37	-7.76	8.07	2.37	-2.72
26.79	7.85	-8.00	9.89	2.57	-2.68
30.81	8.25	-8.27	11.72	2.73	-2.73

TABLE II.- COORDINATES OF THE LEADING-EDGE GLOVES, NORMAL TO THE WING LEADING EDGE - Concluded

Glove 4i		
Leading-edge station 100.00		
x_n	z_{upper}	z_{lower}
-3.76	-3.90	
-3.5	-2.53	-4.28
-3.0	-1.82	-4.55
-2.0	-.78	-4.69
-1.0	.03	-4.62
0	.65	-4.49
2.0	1.61	-4.13
4.0		-3.78
6.0		-3.55
8.0		-3.54
10.0		-3.60

Dimensions are
given in inches

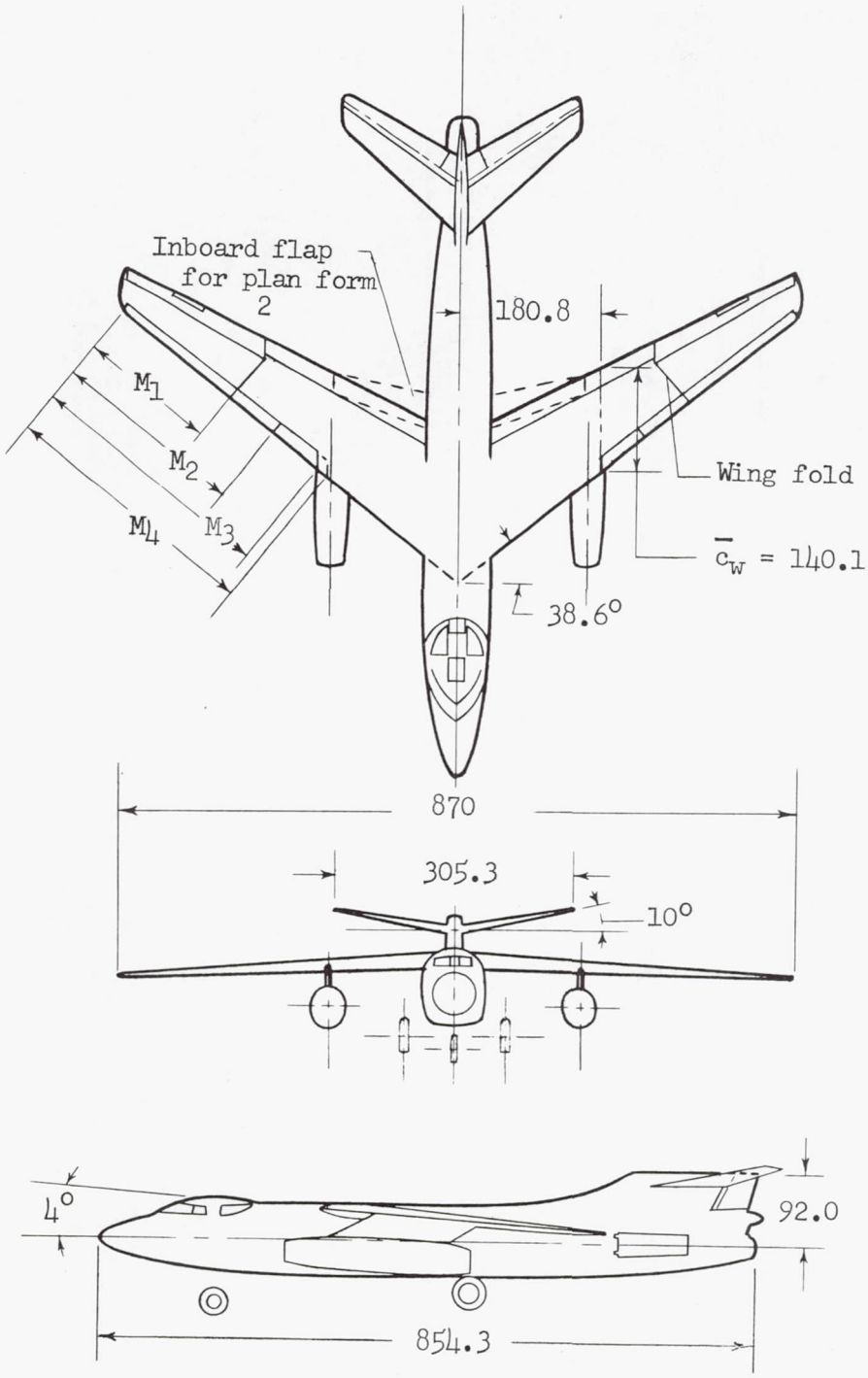

Figure 1.- Three-view sketch of the test airplane.

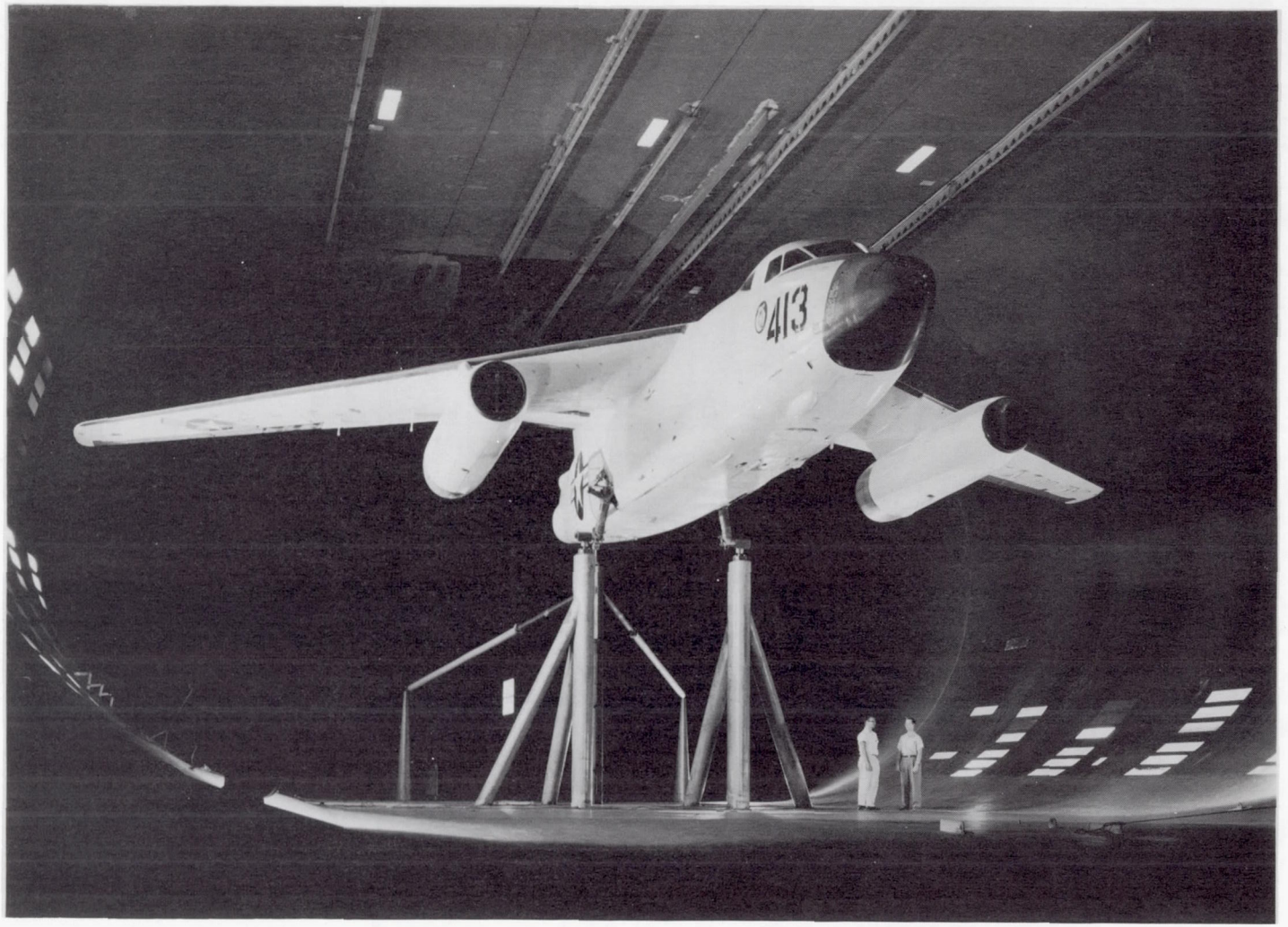

A-20573

Figure 2.- View of the airplane mounted on the struts in the wind tunnel; front view, flaps undeflected.

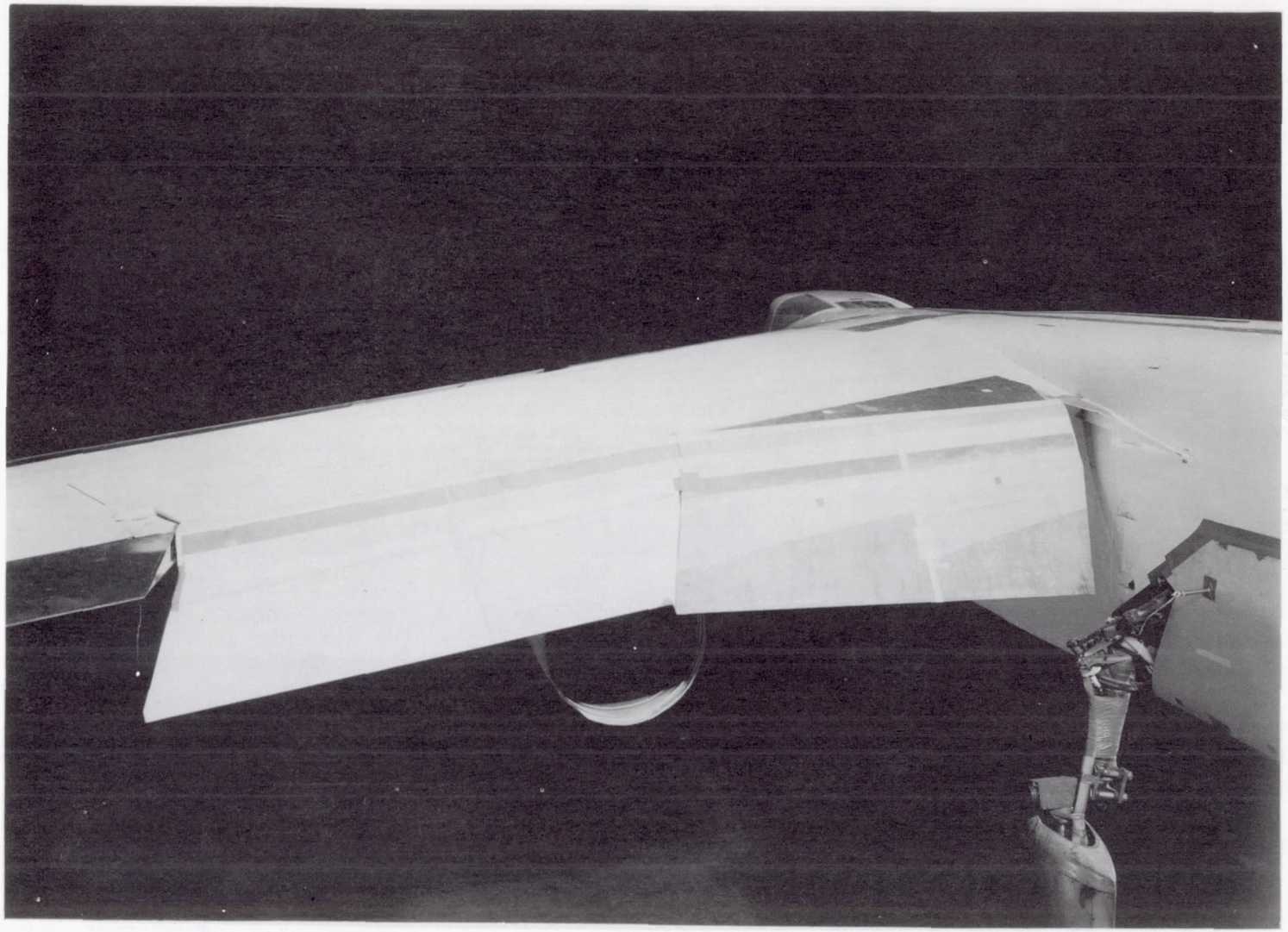

A-21044

Figure 3.- View from behind and above the left wing showing the fillet area of plan form 2.

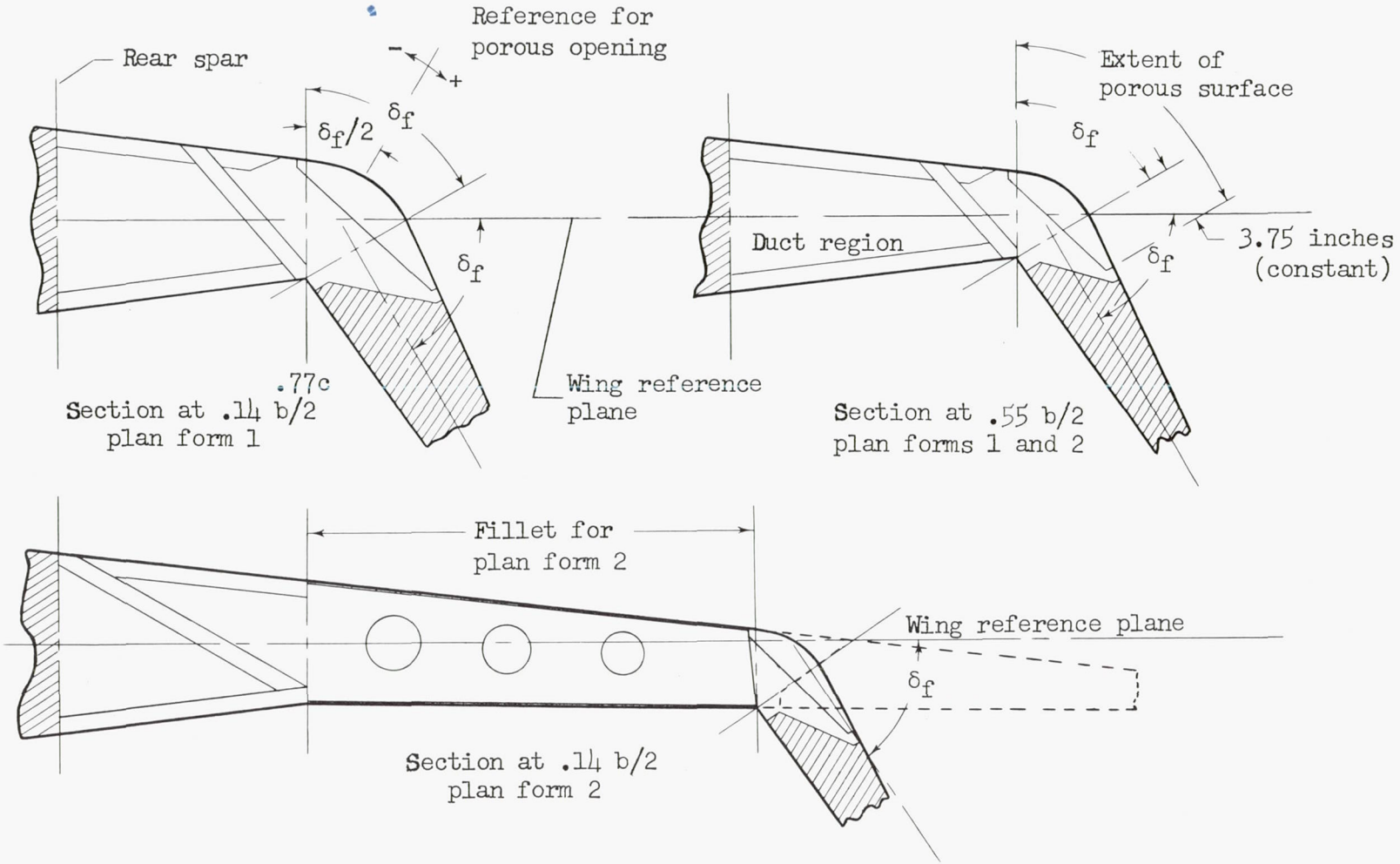

Figure 4.- Profiles of the area-suction flaps.

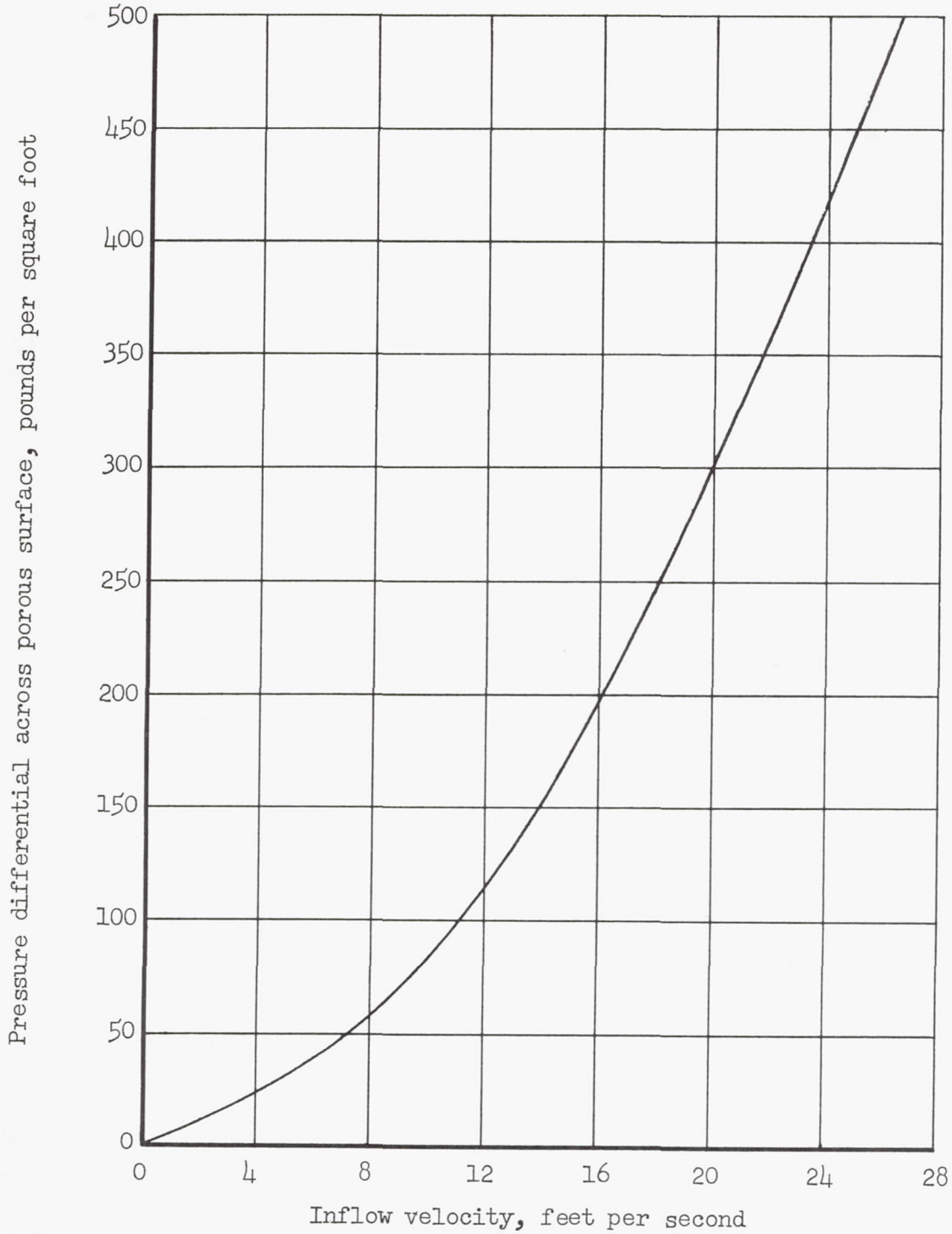

Figure 5.- Flow characteristics of the porous surfaces.

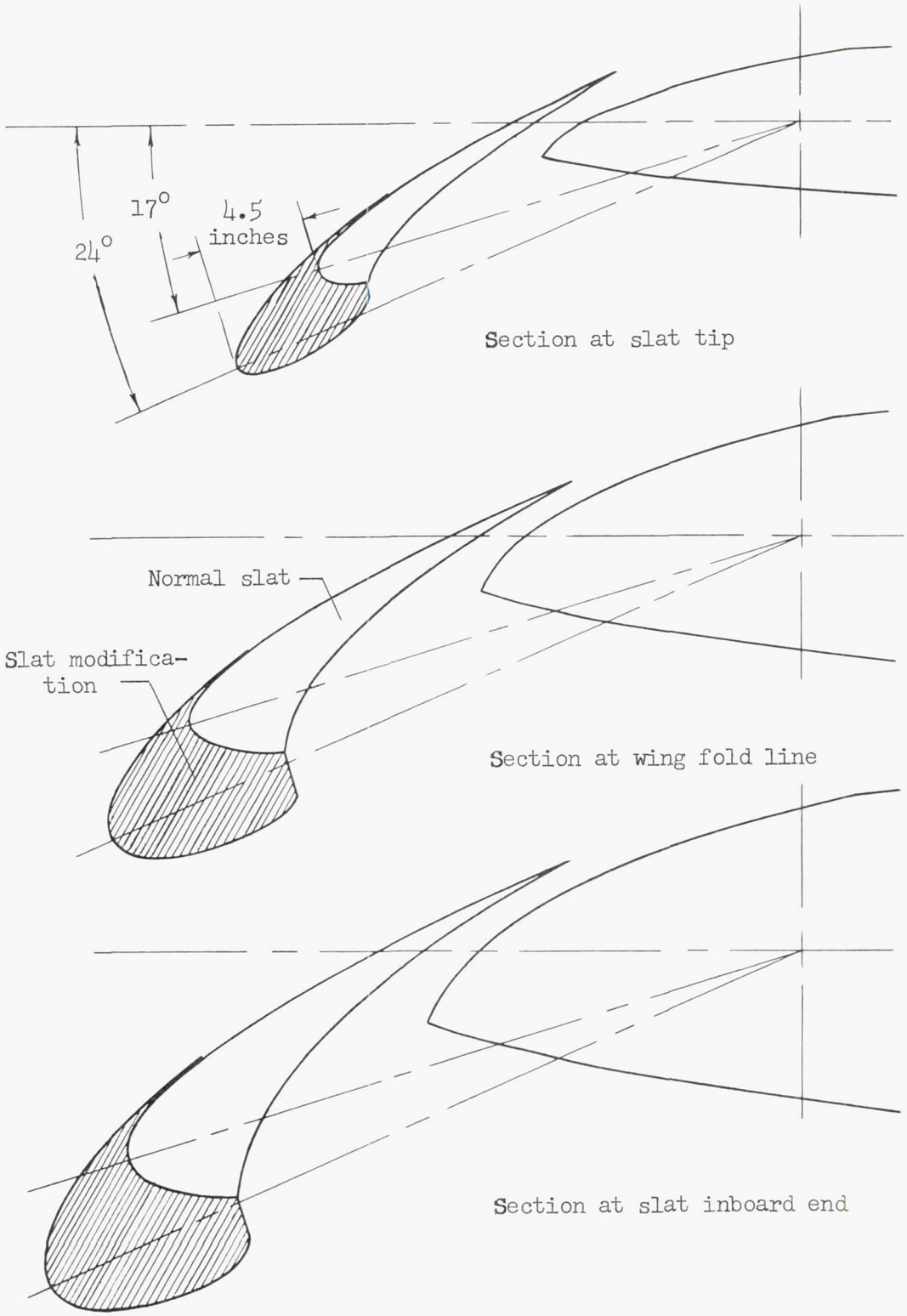

Figure 6.- Contours of the slat modification at various stations.

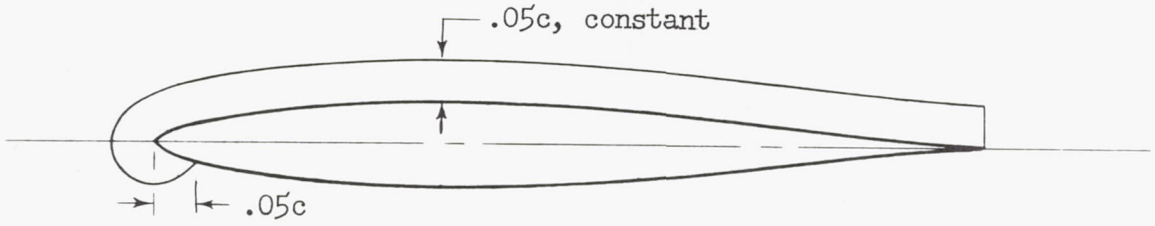

(a) Wing fence.

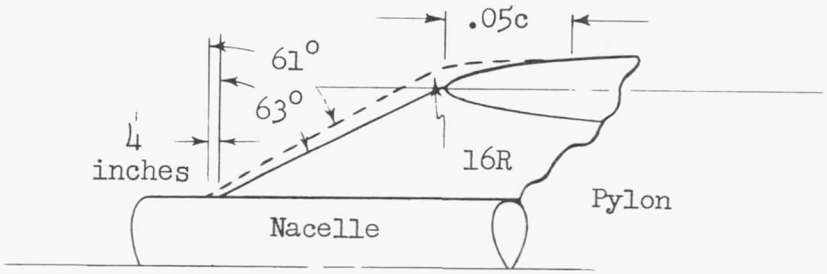

(b) Modified pylon leading edge.

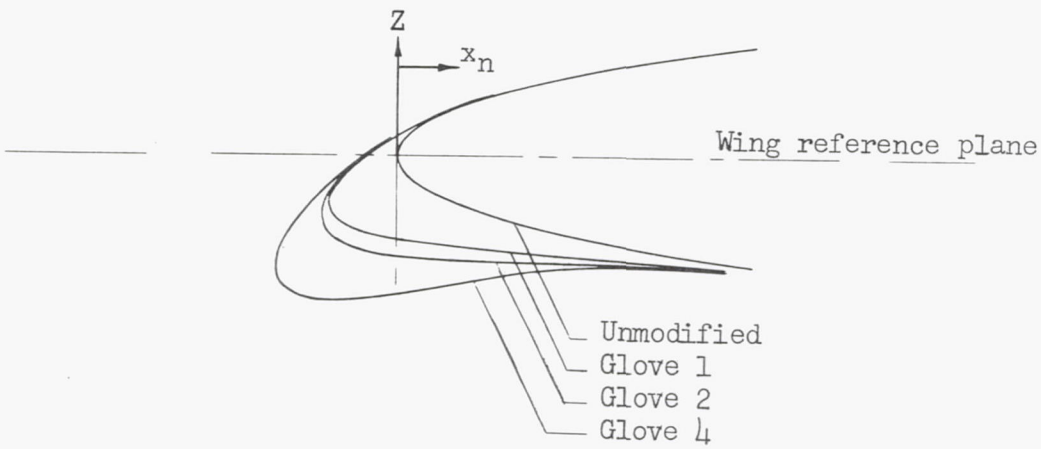

(c) Wing leading-edge gloves.
Typical section normal
to wing leading edge.

Figure 7.- Miscellaneous test devices.

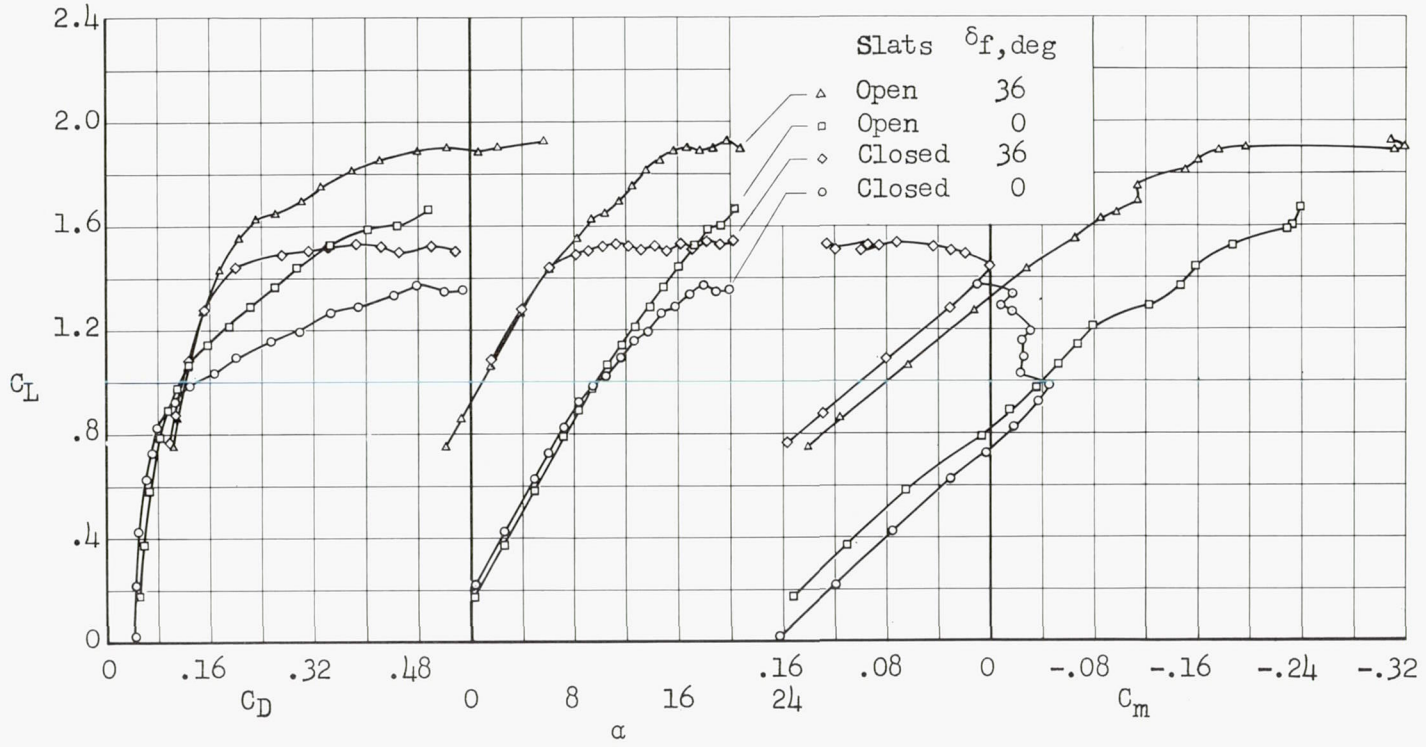

Figure 8.- Aerodynamic characteristics of the complete airplane with plan form 1 and slotted flaps; $R = 8.2 \times 10^6$.

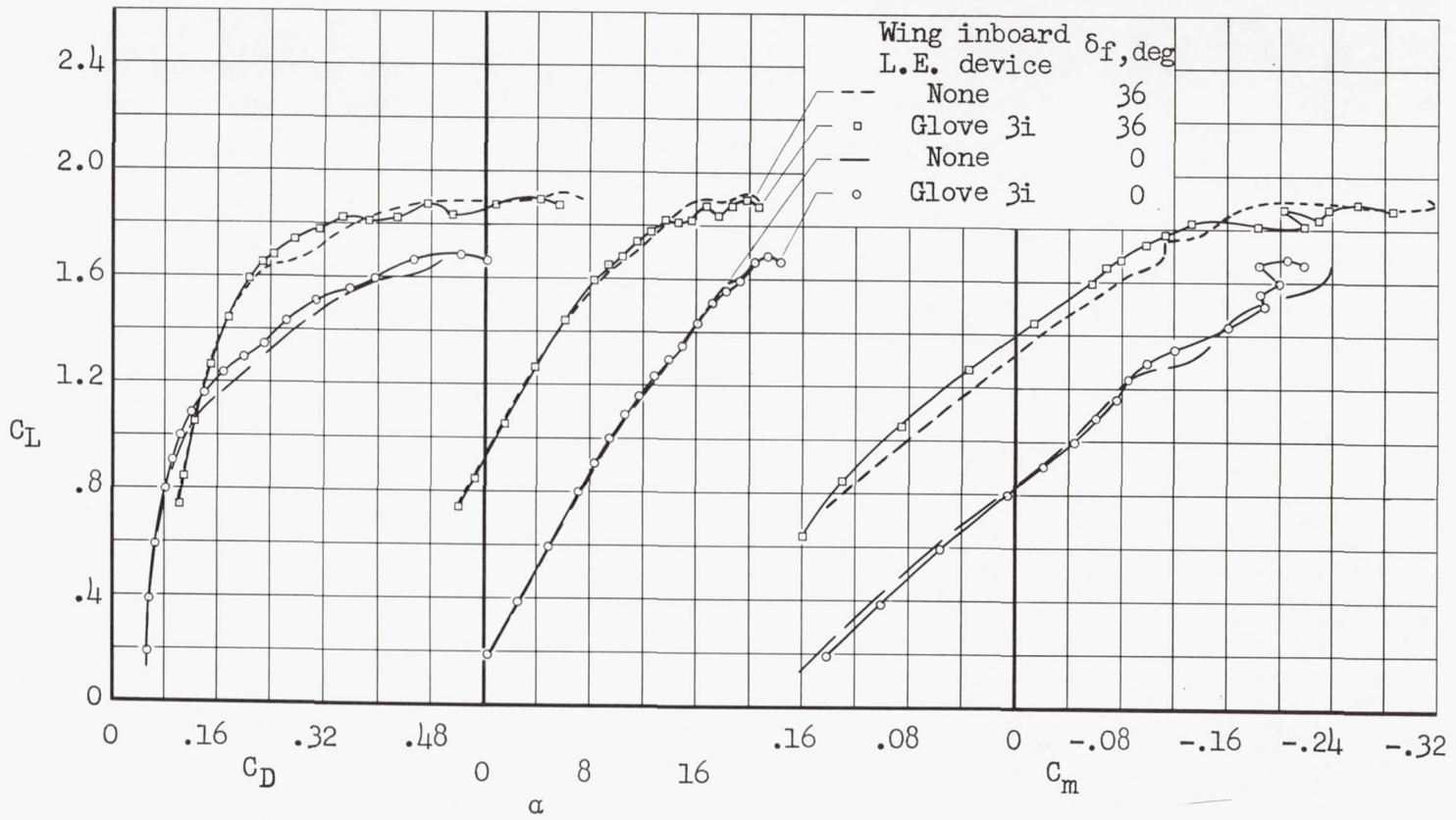

Figure 9.- Effect of an inboard wing leading-edge device on the aerodynamic characteristics of the complete airplane with plan form 1, slats open, and slotted flaps; R = 8.2×10^6.

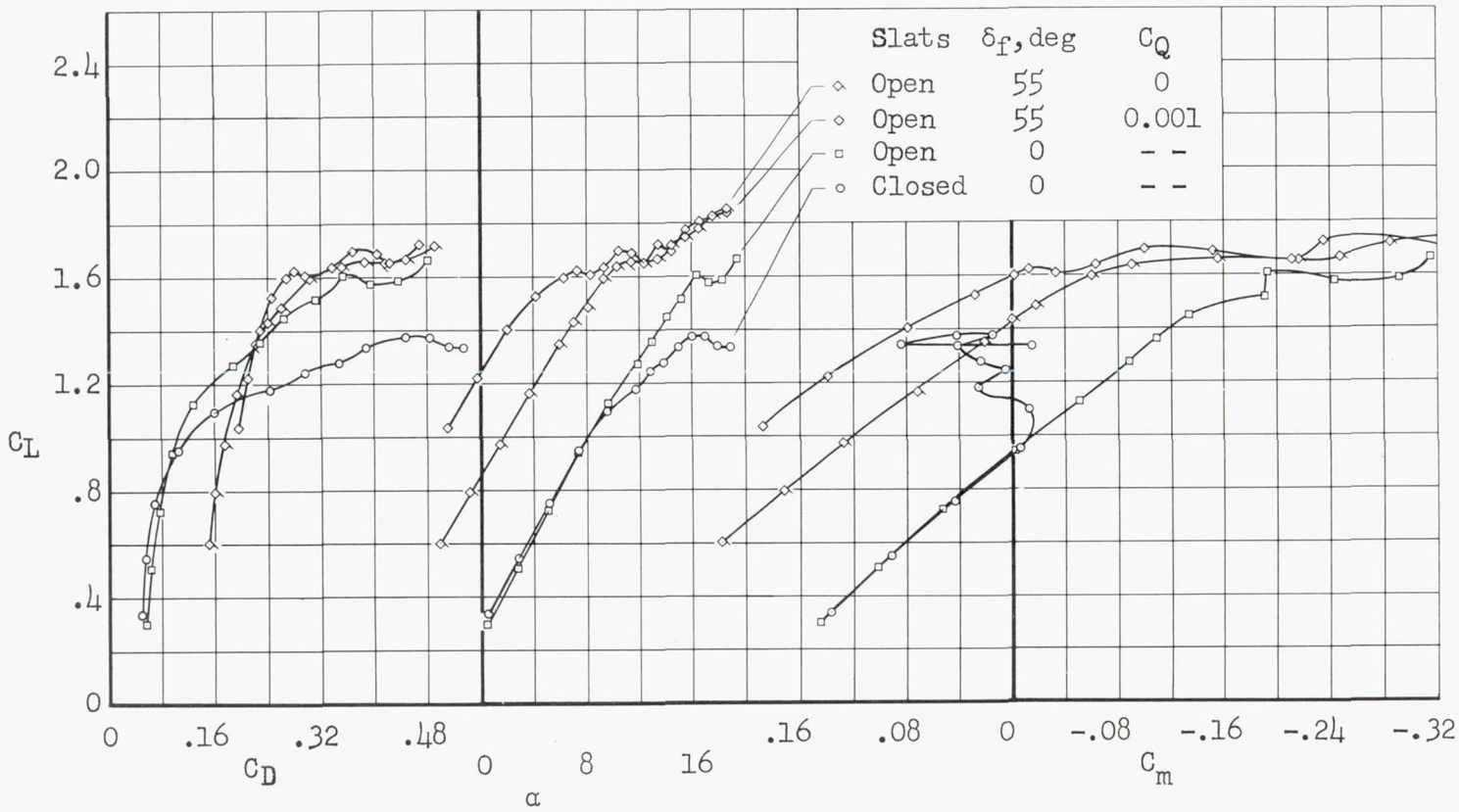

Figure 10.- Aerodynamic characteristics of the complete airplane with plan form 2 and area-suction flaps; R = 8.2×10^6.

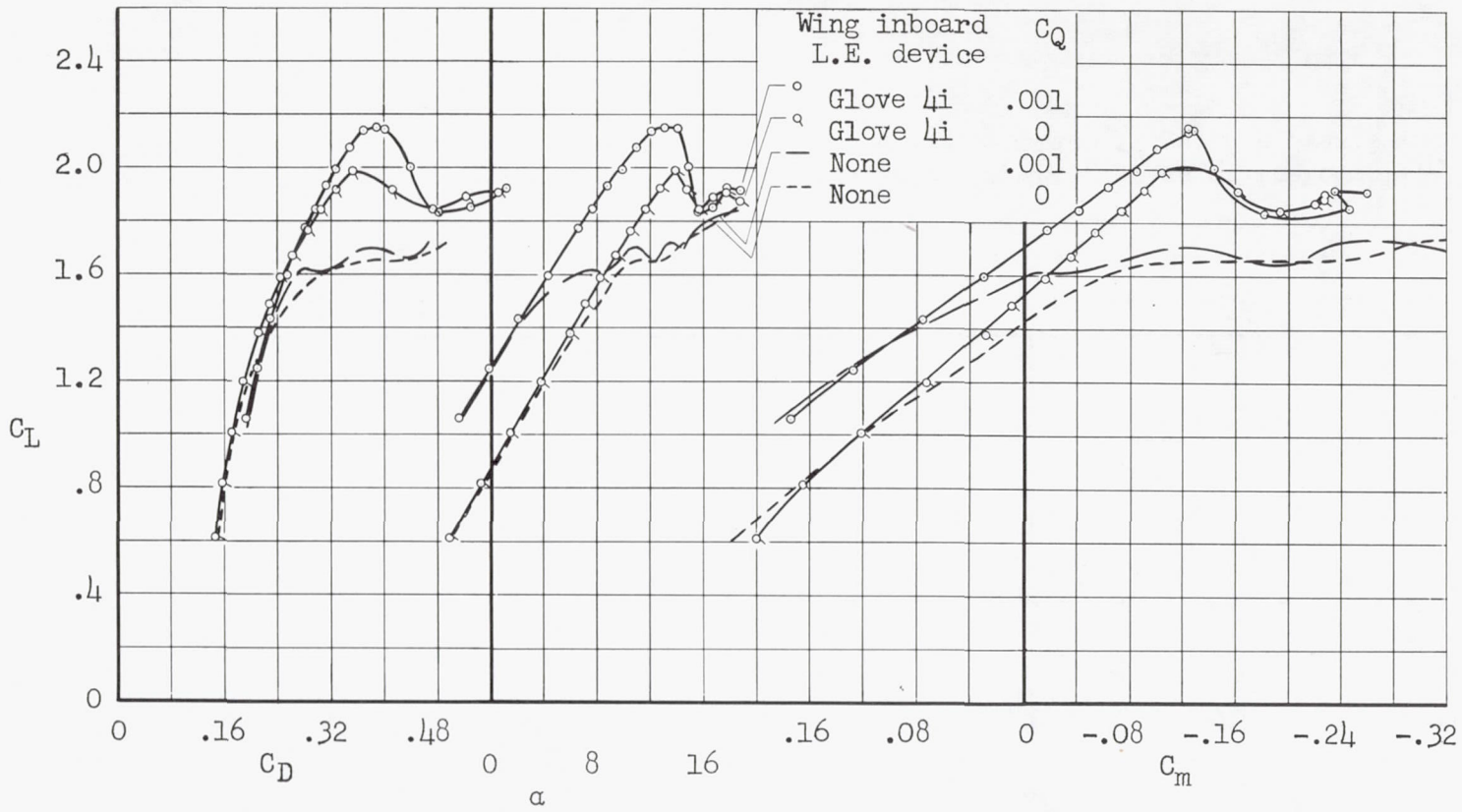

Figure 11.- Effect of a simulated inboard nose flap, glove 4i, on the aerodynamic characteristics of the complete airplane with plan form 2, slats open, and area-suction flaps deflected 55°; $R = 8.2 \times 10^6$.

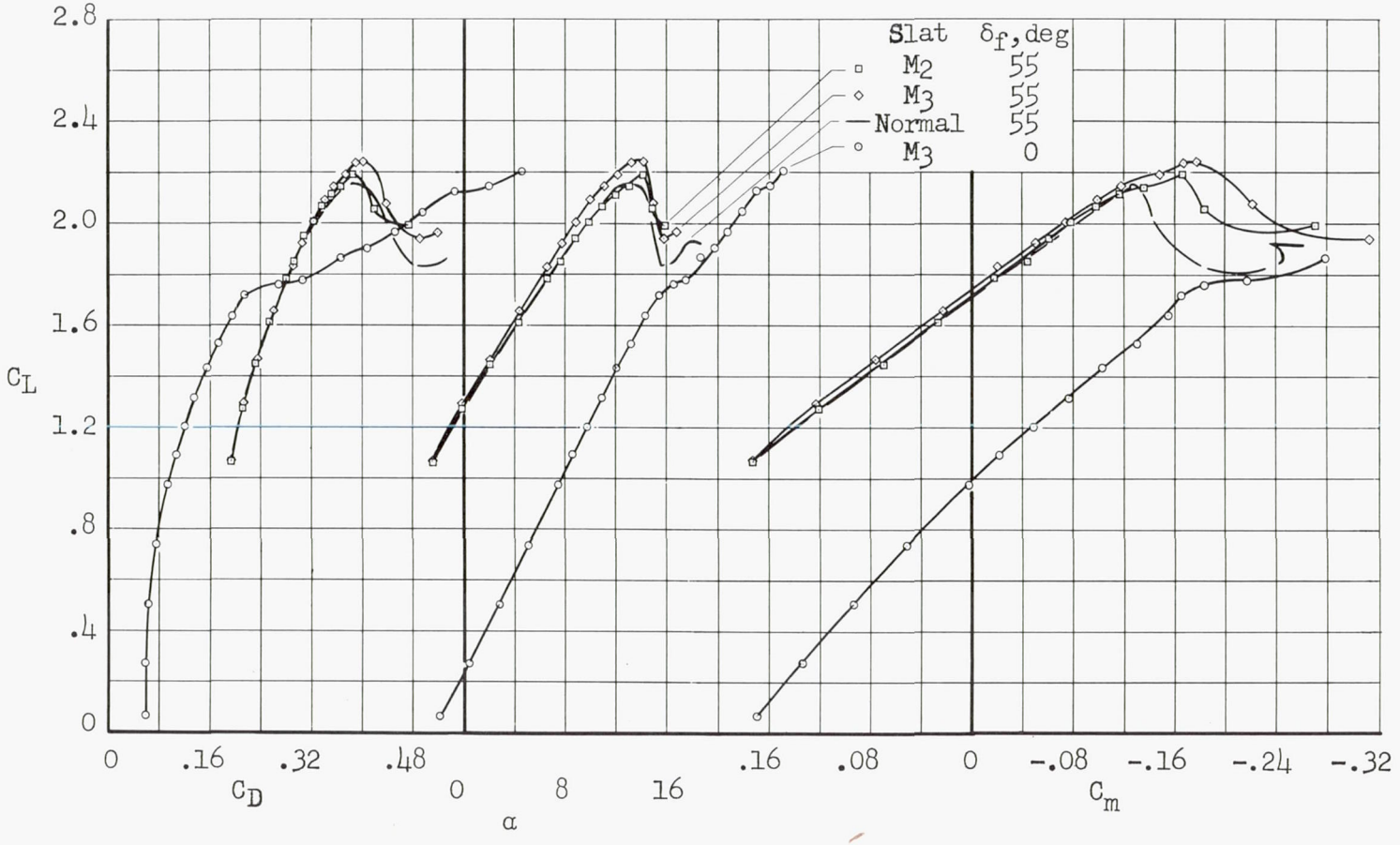

Figure 12.- Effects of slat modifications on the aerodynamic characteristics of the complete airplane with plan form 2, slats open, glove 4i, and area-suction flaps; R = 8.2×10^6.

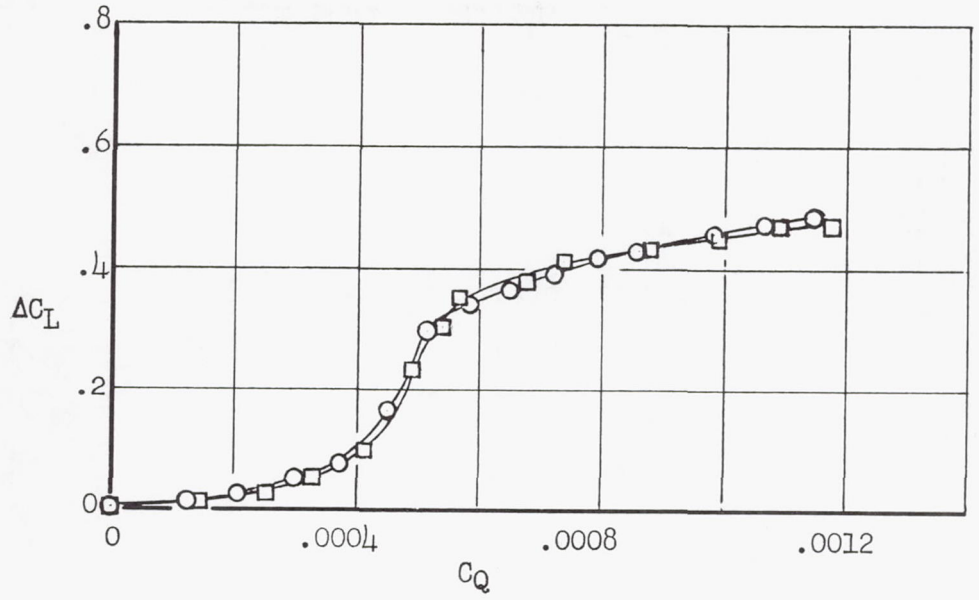

(a) $\alpha = -2.7^\circ$ (av.)

Flap juncture line

○ Unsealed

□ Sealed

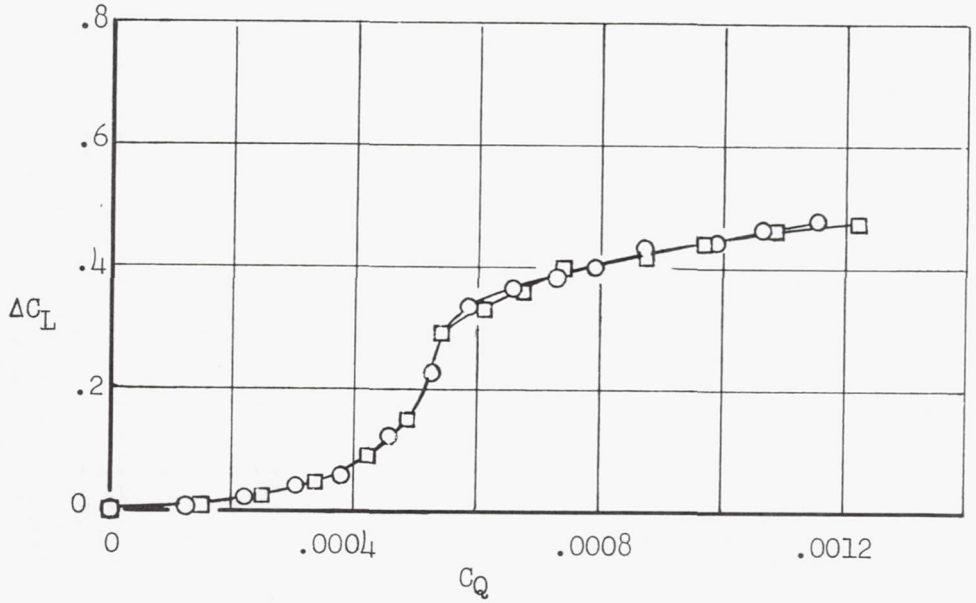

(b) $\alpha = 1.8^\circ$ (av.)

Figure 13.- Variation of the increment of lift due to suction with flow coefficient on plan form 2 with slats M_3, glove 4i, and $\delta_f = 55^\circ$.

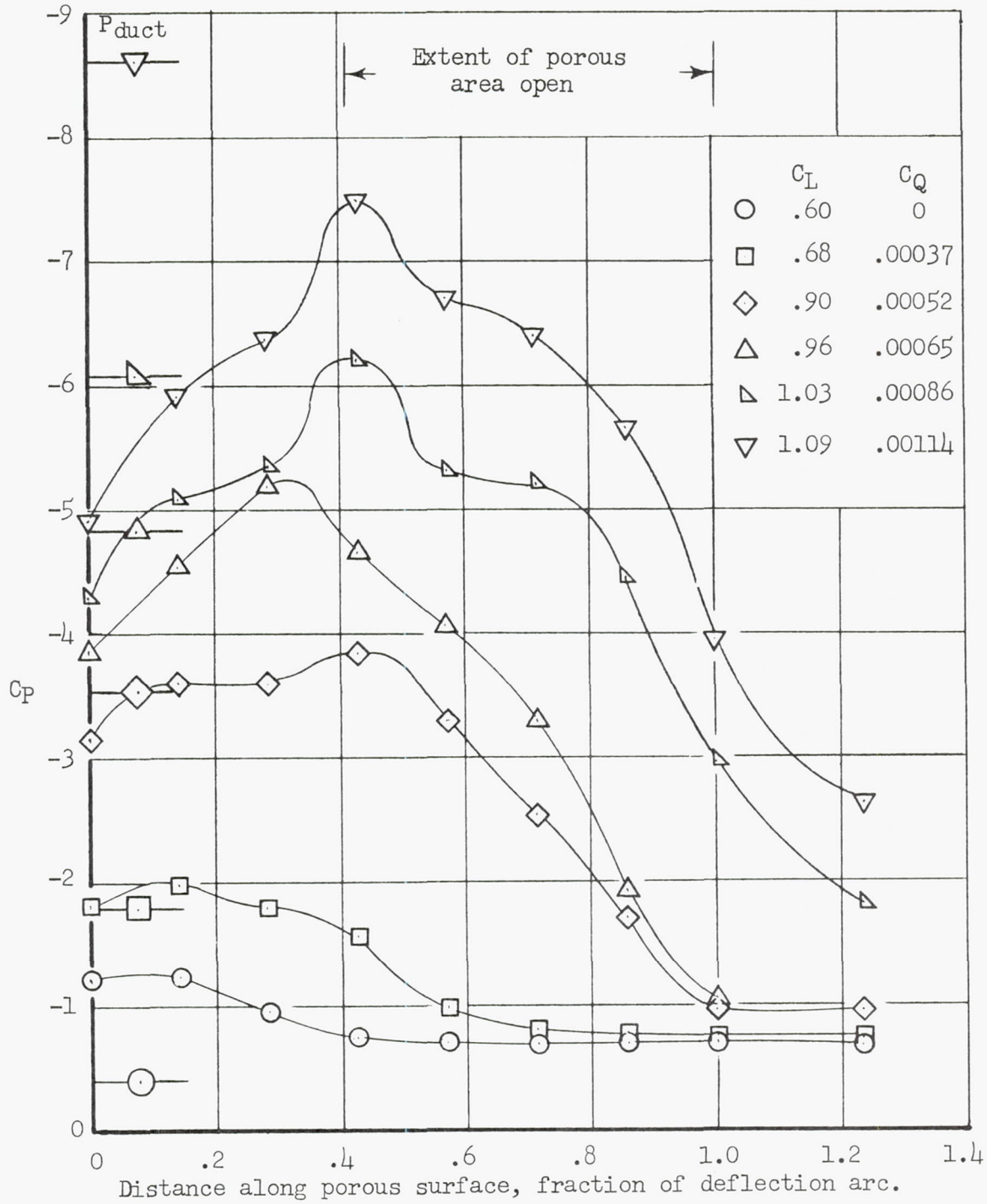

Figure 14.- Pressure distributions over the porous surface at several values of flow coefficient. Plan form 2 with slats M_3, glove 4i, and area-suction flaps deflected 55°; α = -2.7°(av.); R = 8.2×10^6.

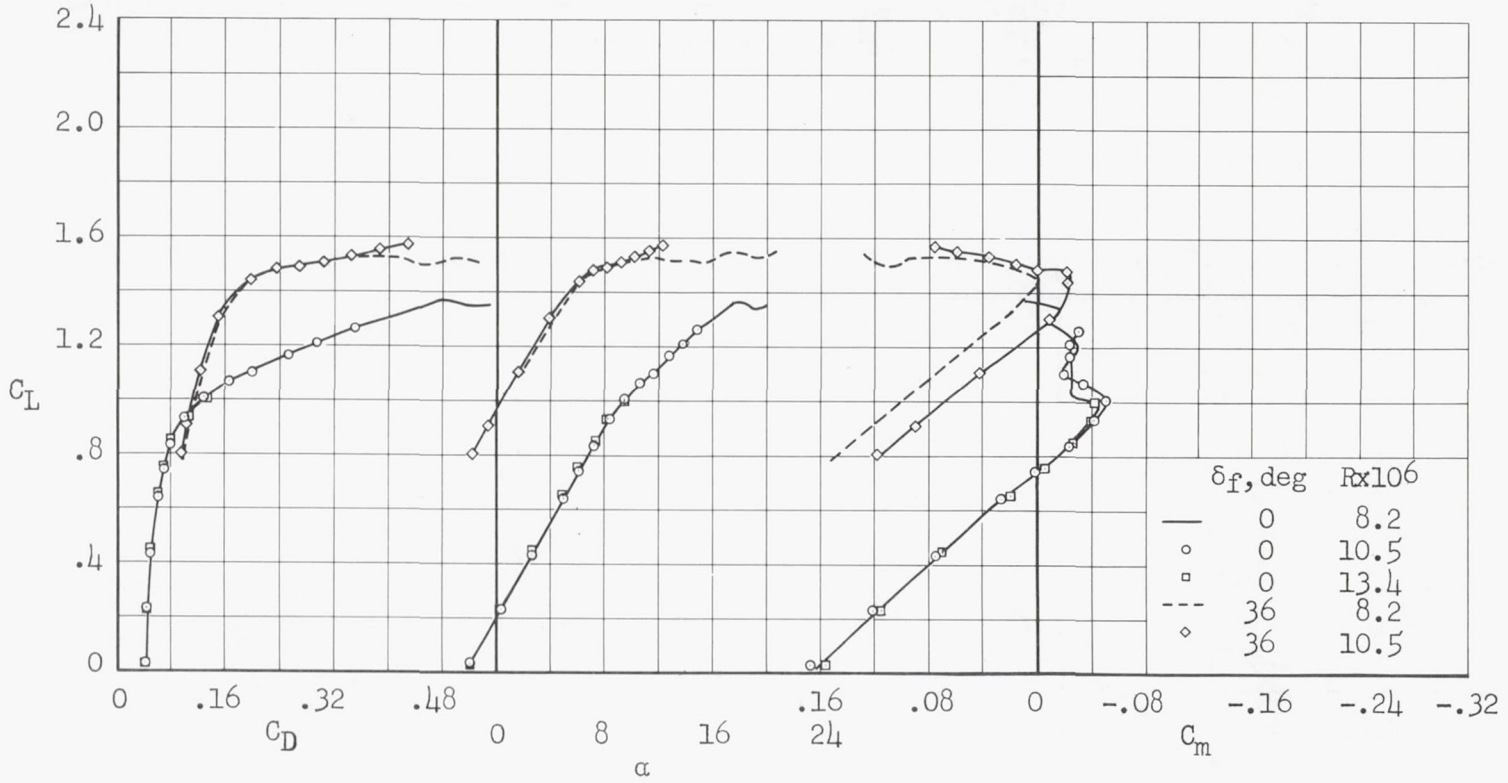

(a) Slats closed.

Figure 15.- Reynolds number effects on the aerodynamic characteristics of the complete airplane with plan form 1 and slotted flaps.

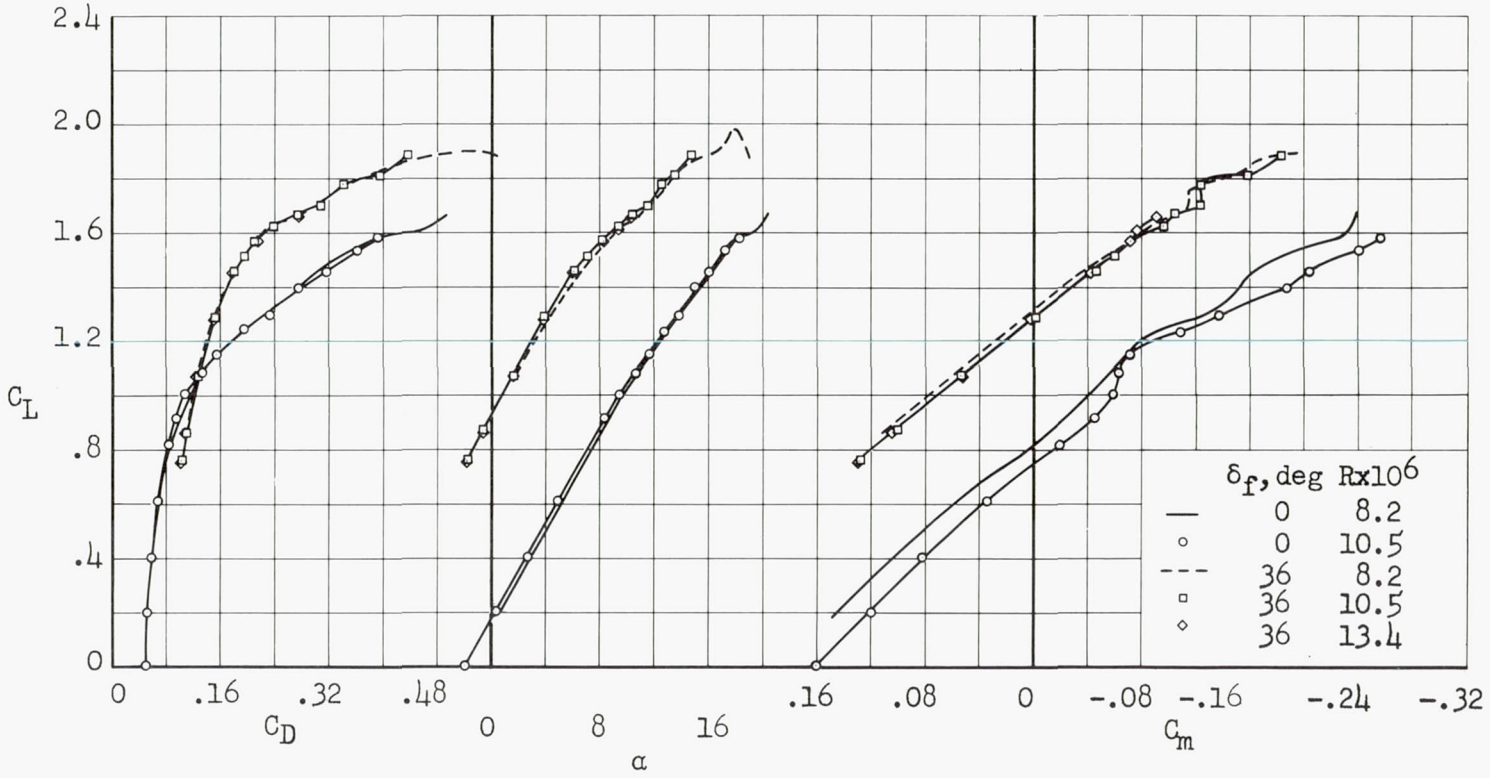

(b) Slats open.

Figure 15.- Concluded.

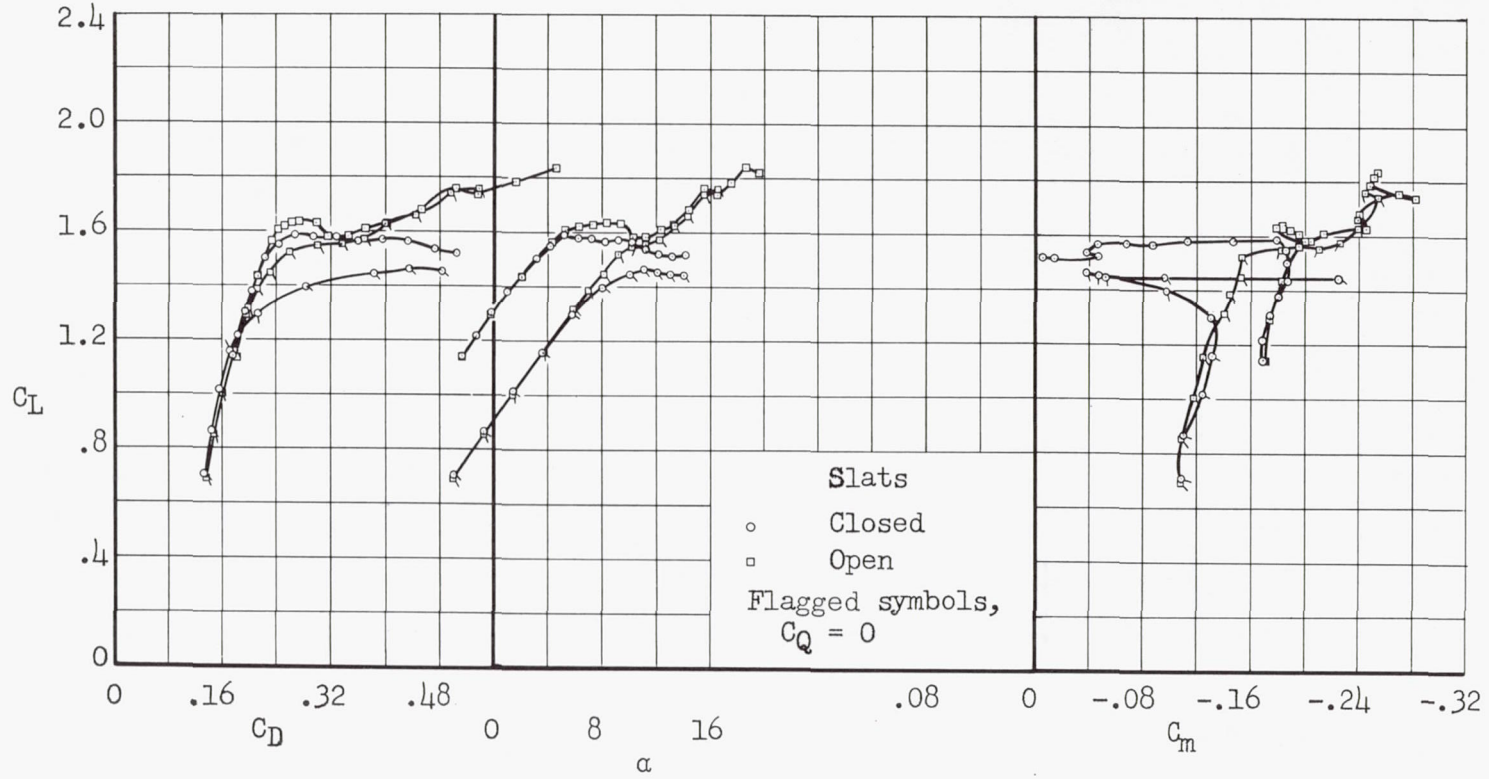

Figure 16.- Effect of slats on the aerodynamic characteristics of the airplane with plan form 1 and area-suction flaps deflected 55°; horizontal tail off; R = 8.2×10^6.

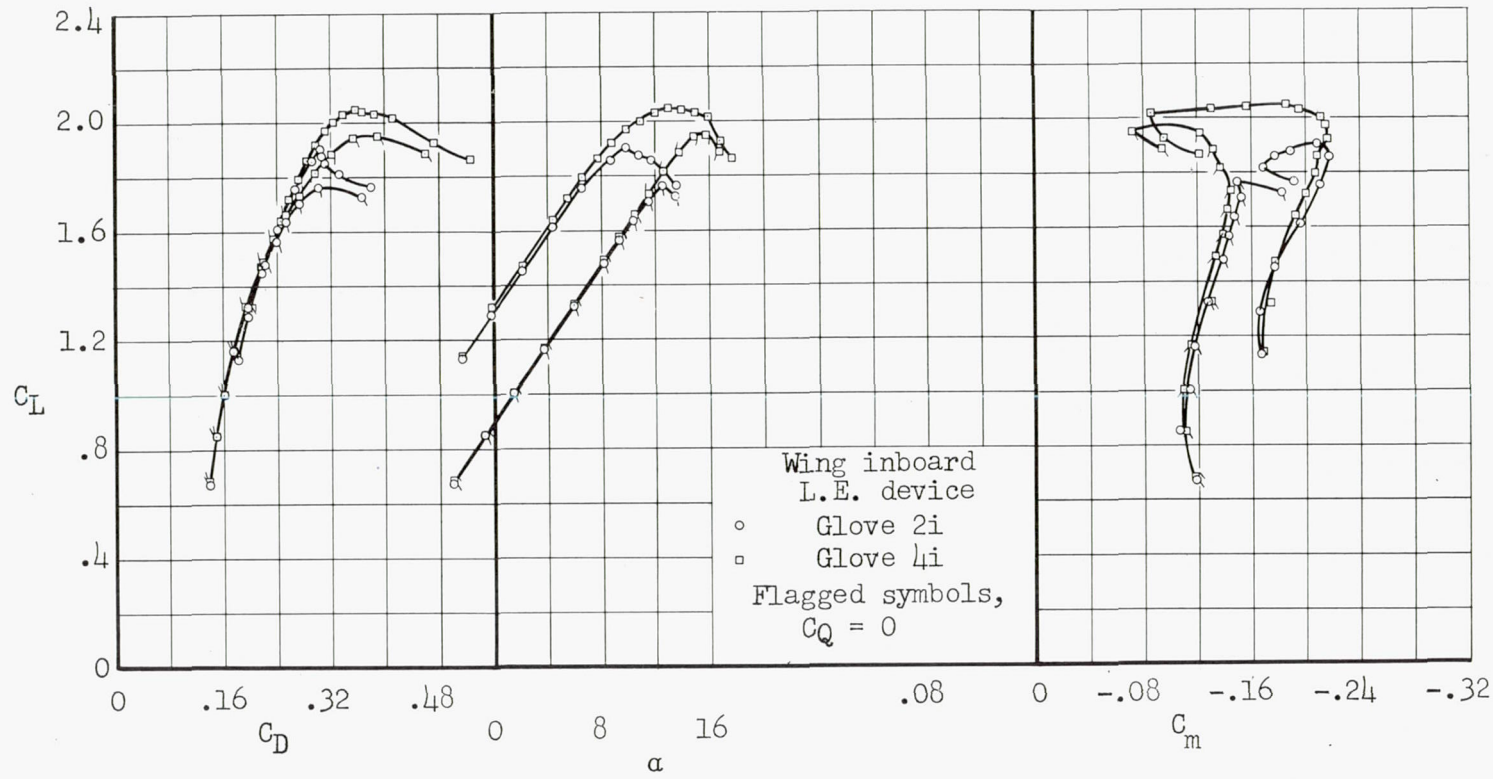

Figure 17.- Effects of inboard wing leading-edge devices on the aerodynamic characteristics of the airplane with plan form 1, slats open, and area-suction flaps deflected 55°; horizontal tail off; R = 8.2×10^6.

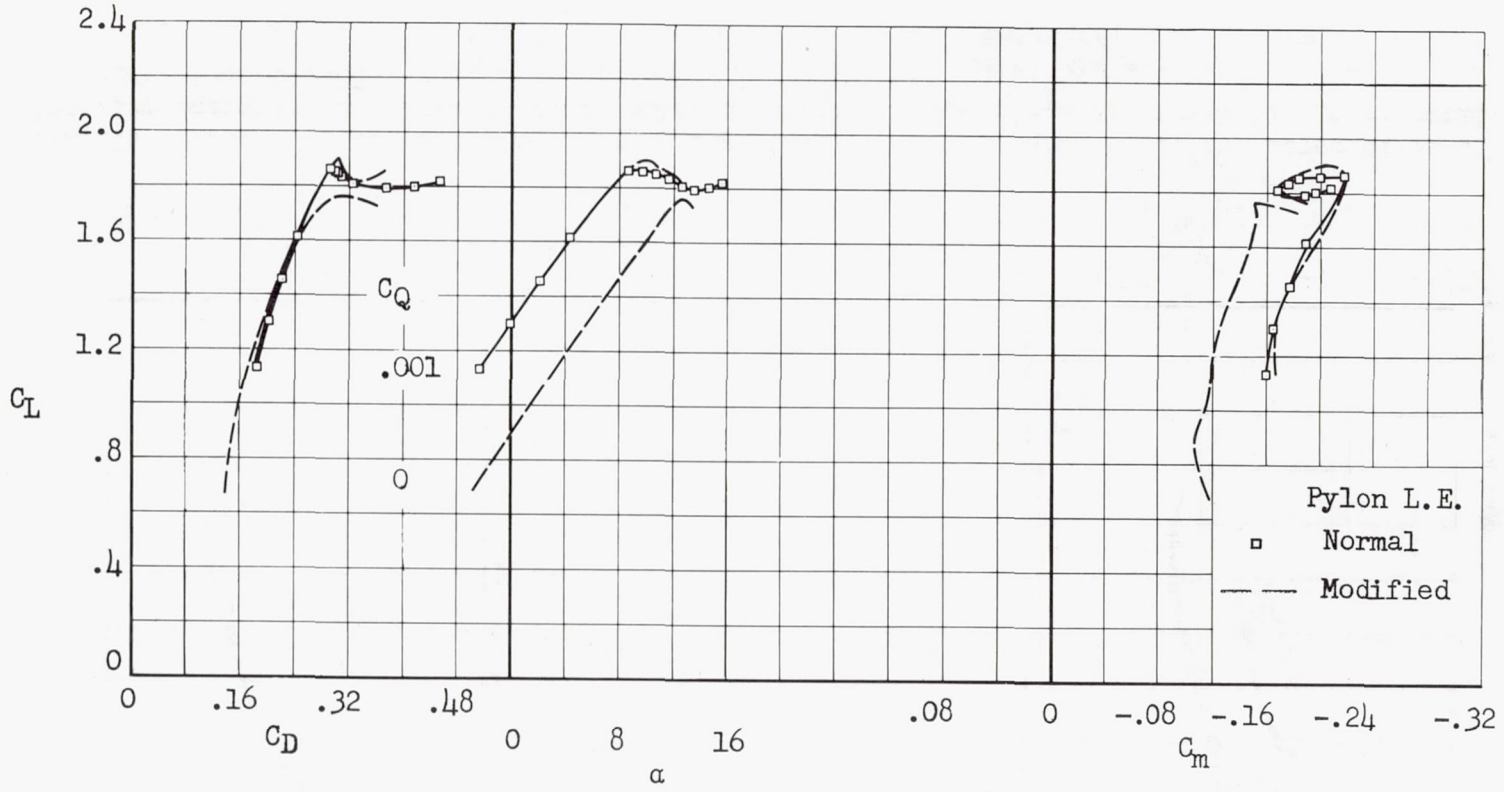

Figure 18.- Effect of a pylon leading-edge change on the aerodynamic characteristics of the airplane with plan form 1, slats open, glove 2i, and area-suction flaps deflected 55°; horizontal tail off; $R = 8.2 \times 10^6$.

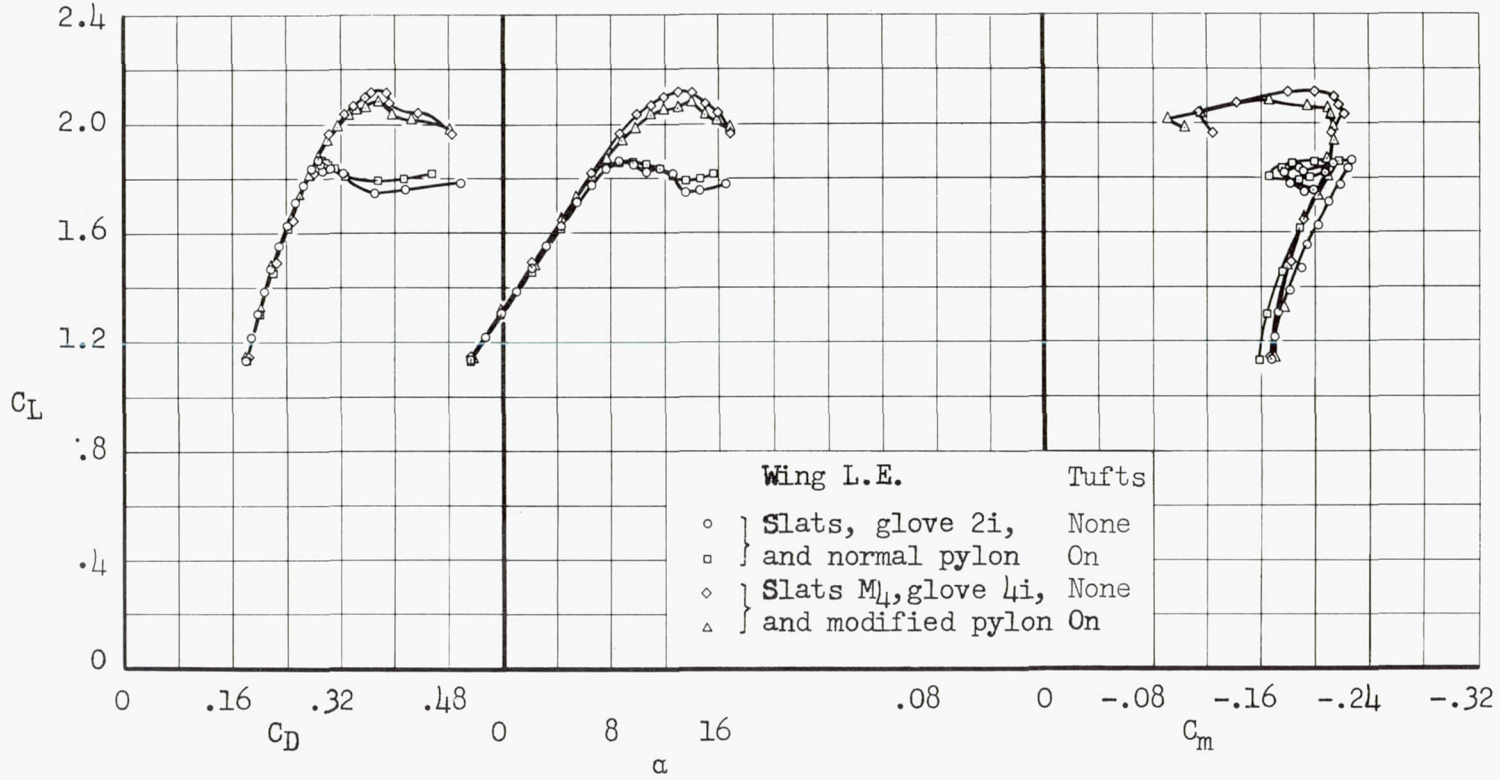

Figure 19.- Effects of tufts on the aerodynamic characteristics of the airplane with plan form 1 and area-suction flaps deflected 55°; horizontal tail off; R = 8.2×10^6.

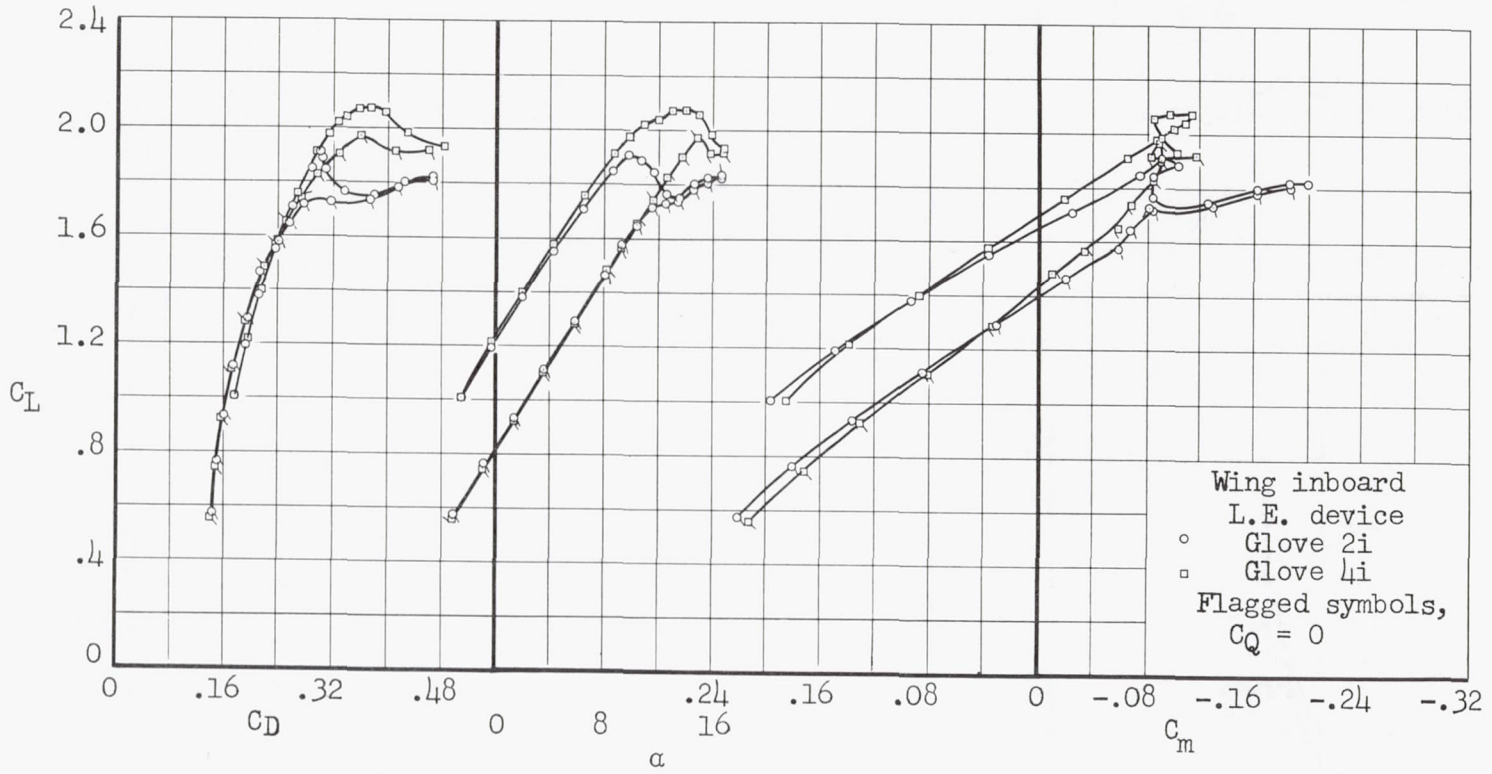

Figure 20.- Effects of inboard wing leading-edge devices on the aerodynamic characteristics of the complete airplane with plan form 1, slats open, and area-suction flaps deflected 55°; R = 8.2×10^6.

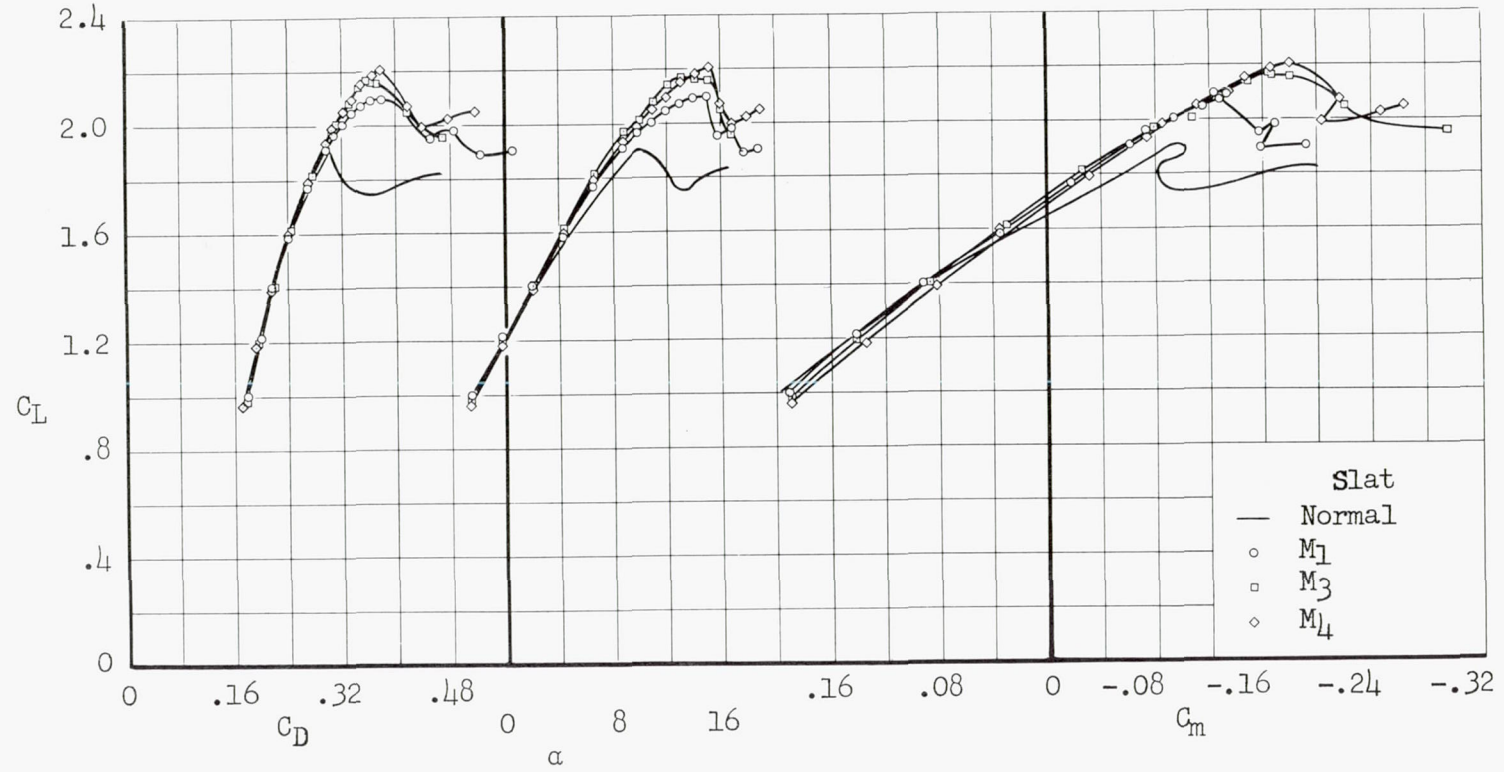

Figure 21.- Effects of slat modifications on the aerodynamic characteristics of the complete airplane with plan form 1, glove 4i, and area-suction flaps deflected 55°; R = 8.2×10^6.

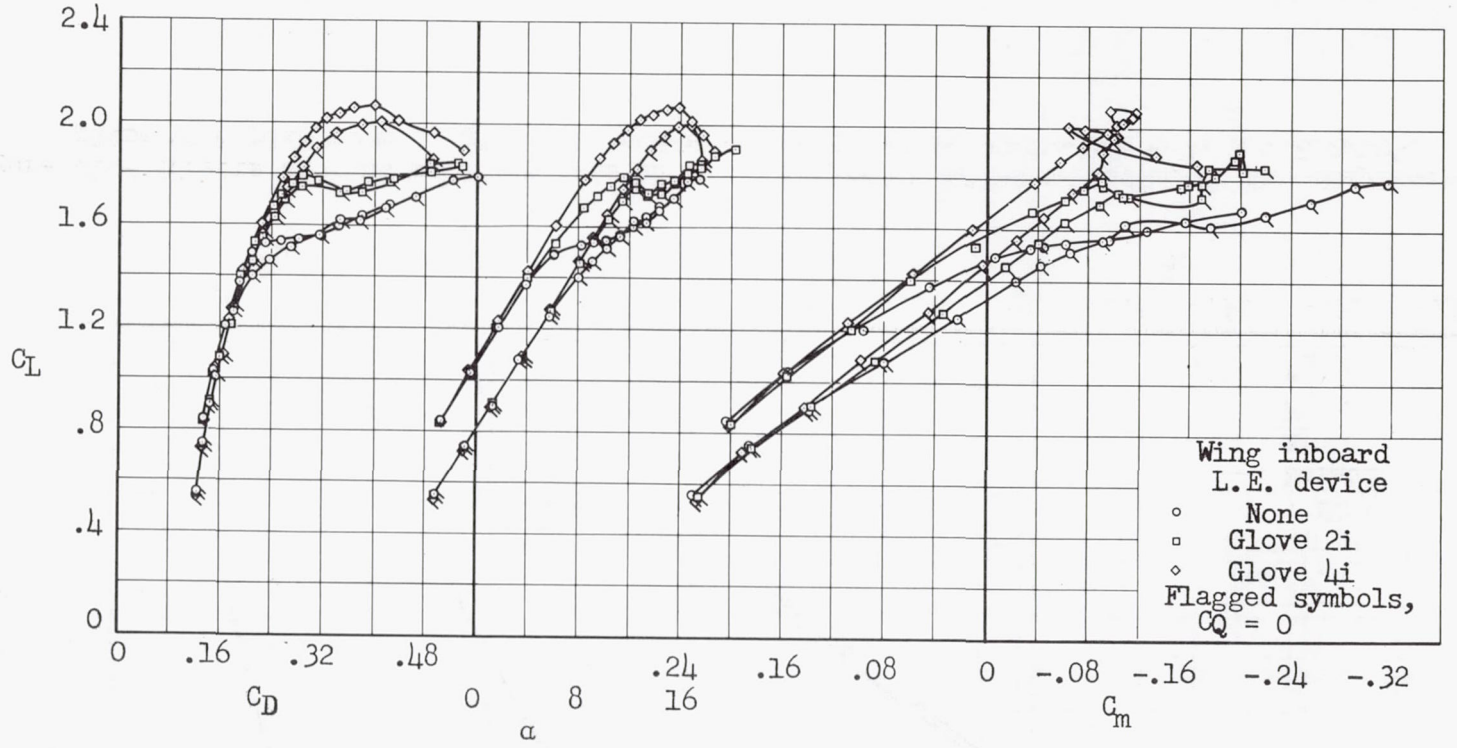

Figure 22.- Effects of inboard wing leading-edge devices on the aerodynamic characteristics of the complete airplane with plan form 1, slats open, and area-suction flaps deflected 45°; $R = 8.2 \times 10^6$.

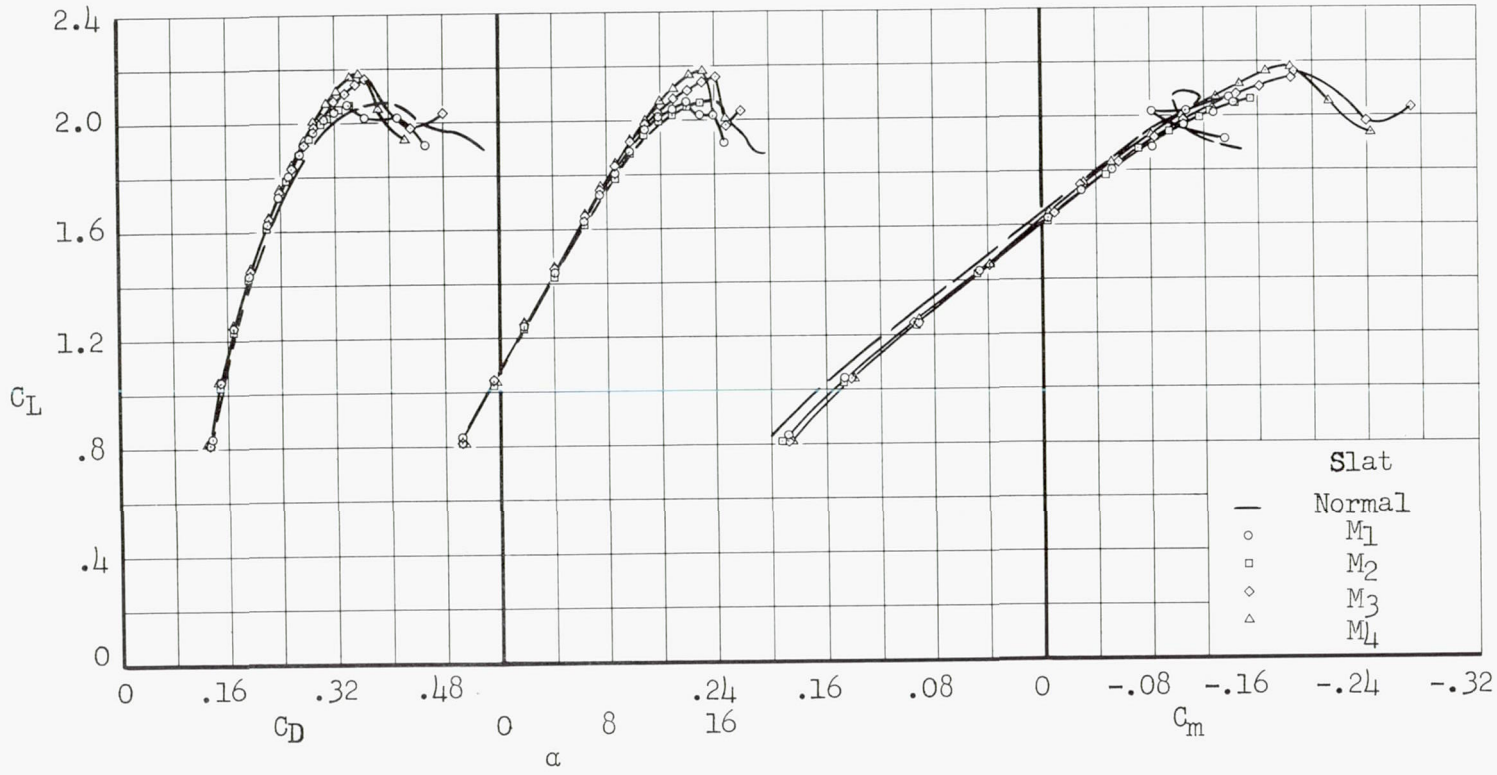

Figure 23.- Effect of slat modifications on the aerodynamic characteristics of the complete airplane with plan form 1, glove 4i, and area-suction flaps deflected 45°; $R = 8.2 \times 10^6$.

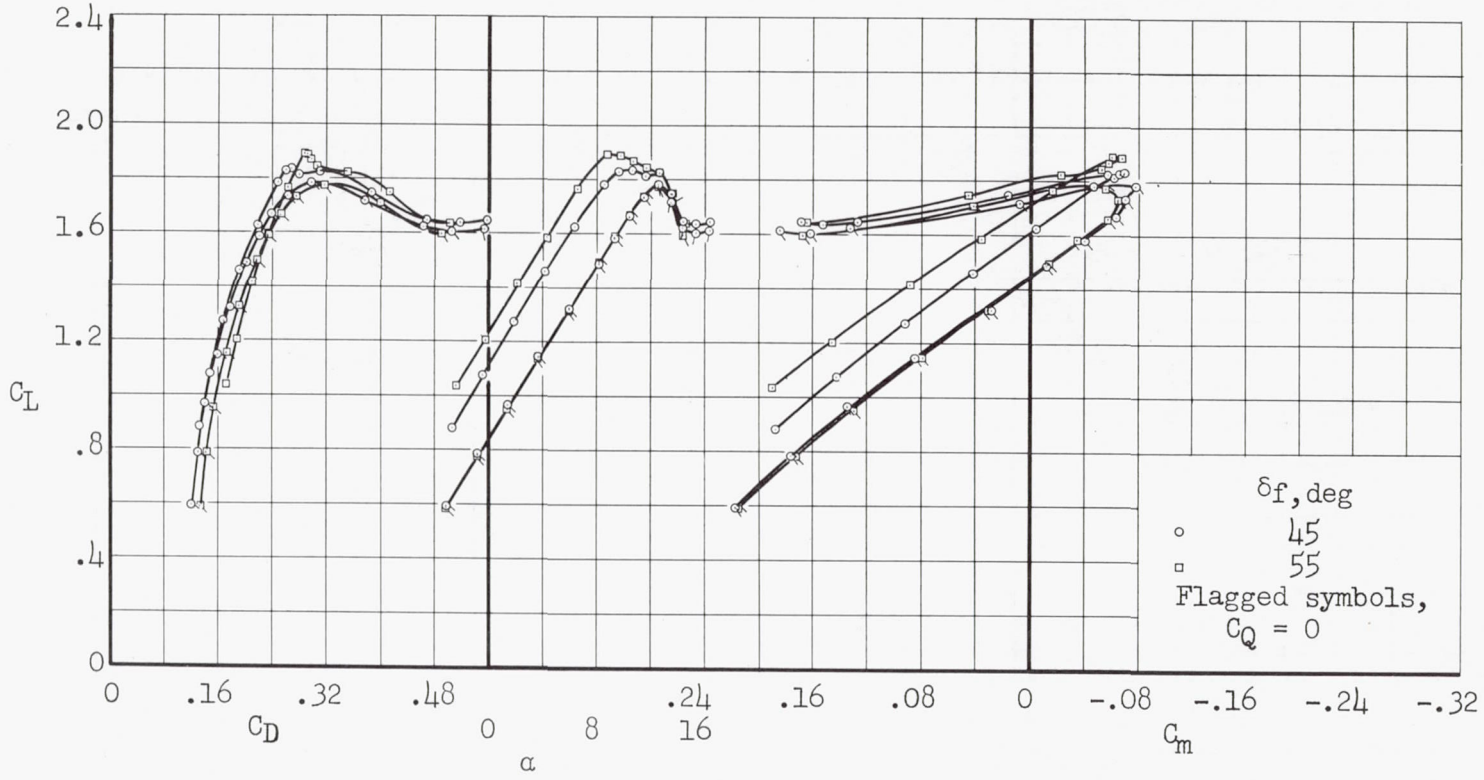

Figure 24.- Aerodynamic characteristics of the complete airplane with plan form 1, glove 2, slats closed, and area-suction flaps; R = 8.2×10^6.

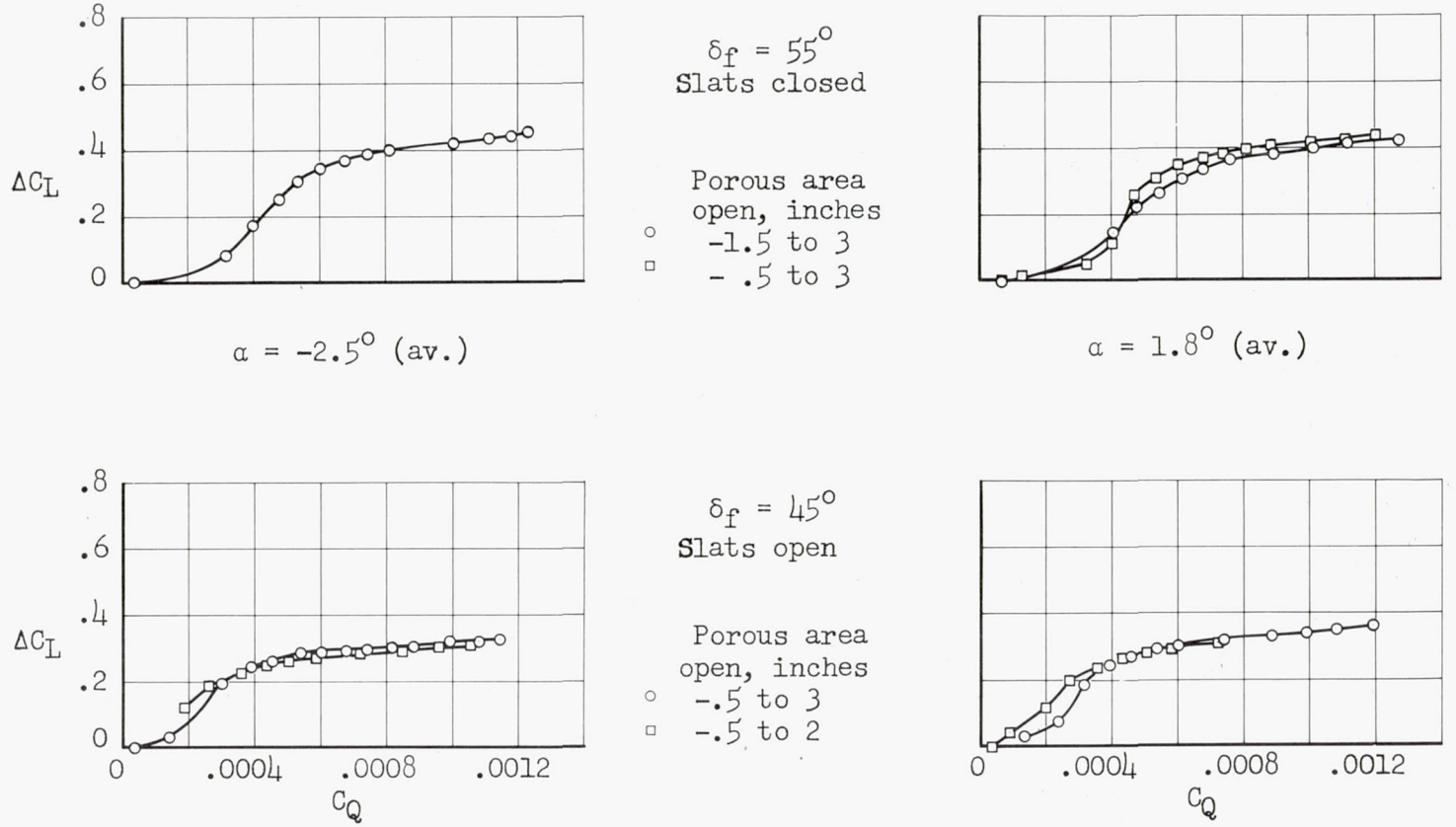

(a) Effect of changes in chordwise extent of porous area open.

Figure 25.- Influence of suction-flow coefficient on lift and pressure distribution for several configurations on plan form 1.

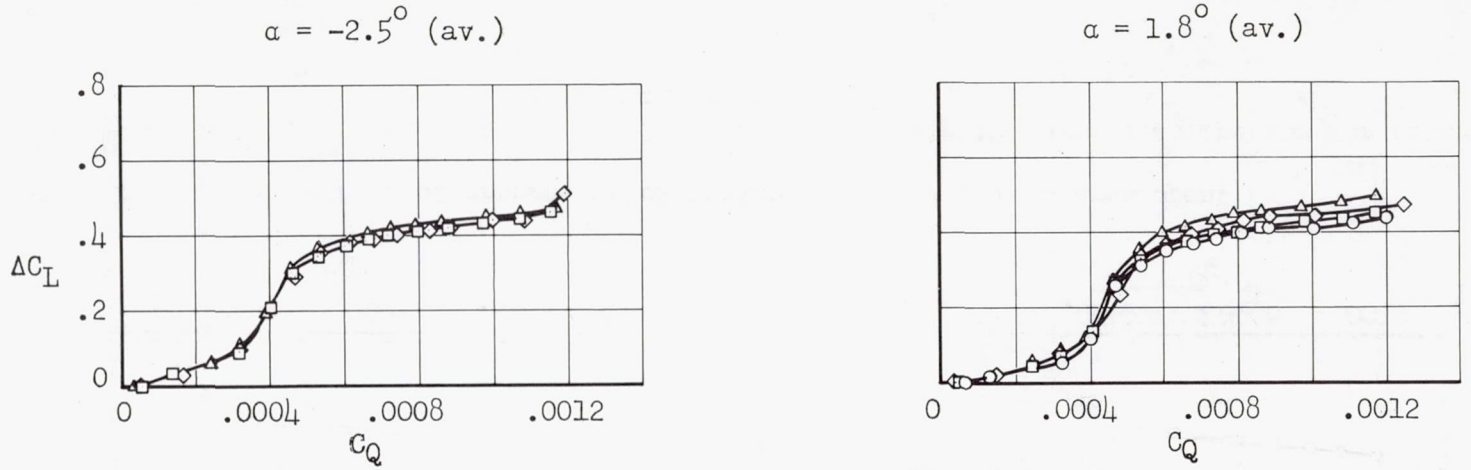

(b) Effect of changes in wing leading-edge configuration; $\delta_f = 55°$.

Figure 25.- Continued.

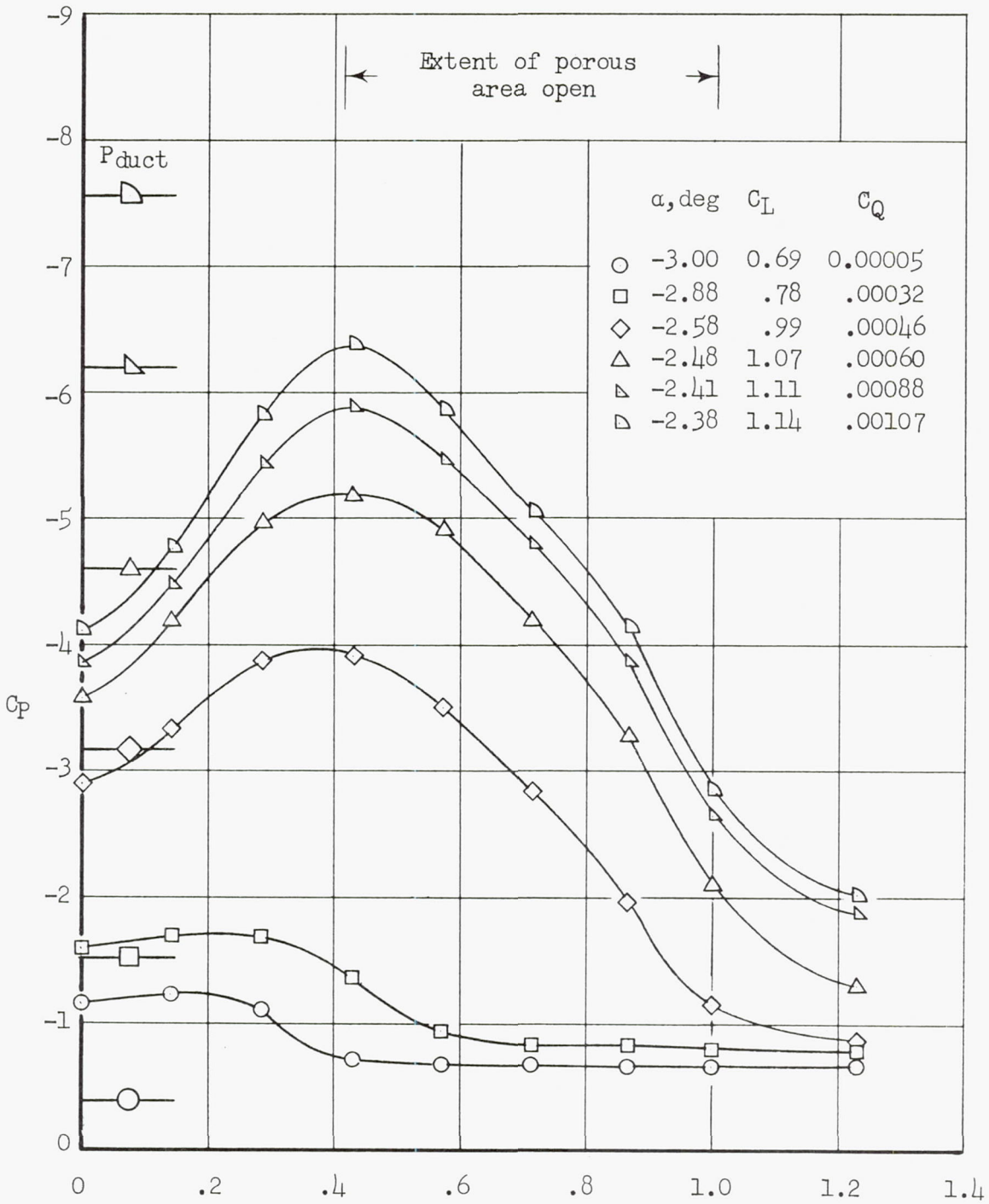

(c) Pressure distributions over the porous surface at several values of flow coefficient; slats open; $\delta_f = 55^\circ$.

Figure 25.- Concluded.

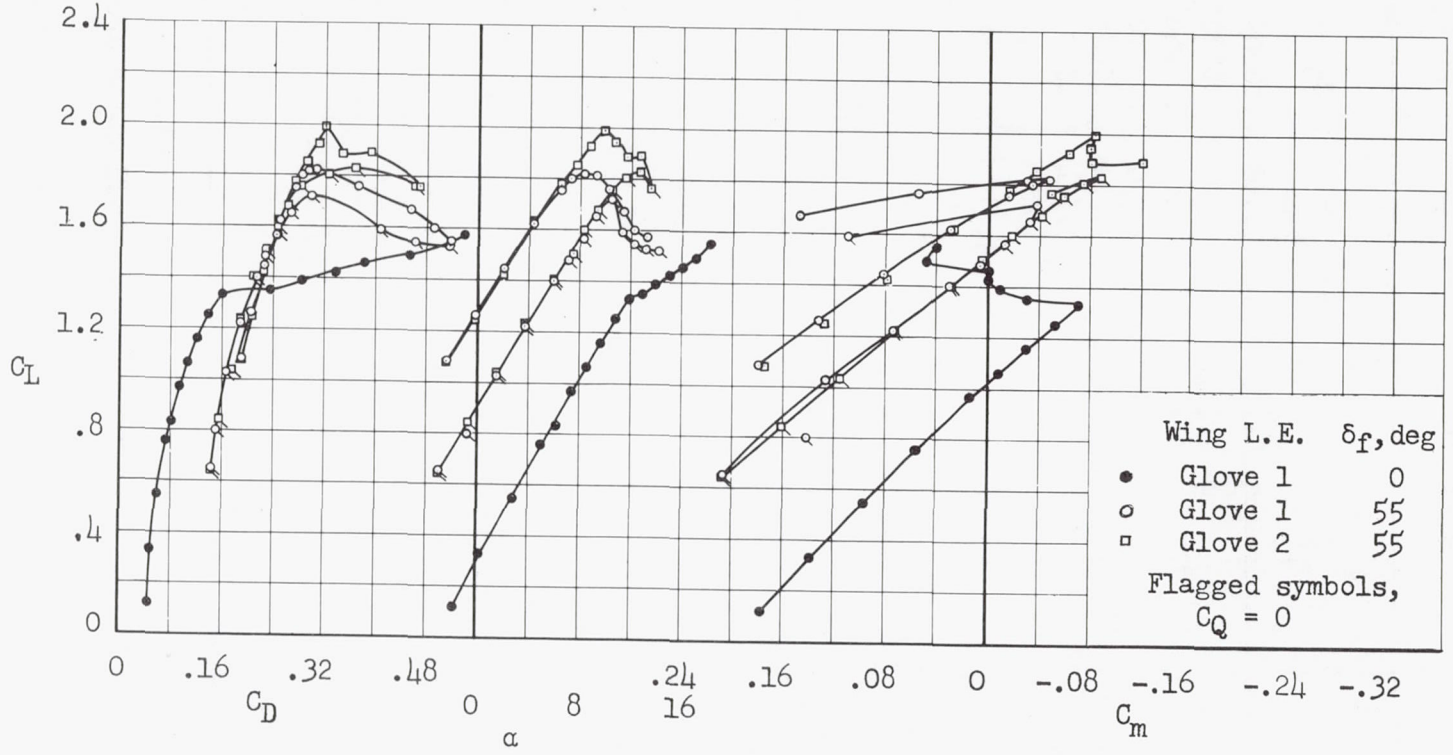

Figure 26.- Effects of wing leading-edge camber and bluntness (gloves 1 and 2) on the aerodynamic characteristics of the complete airplane with plan form 2, slats closed, and area-suction flaps; R = 8.2×10^6.

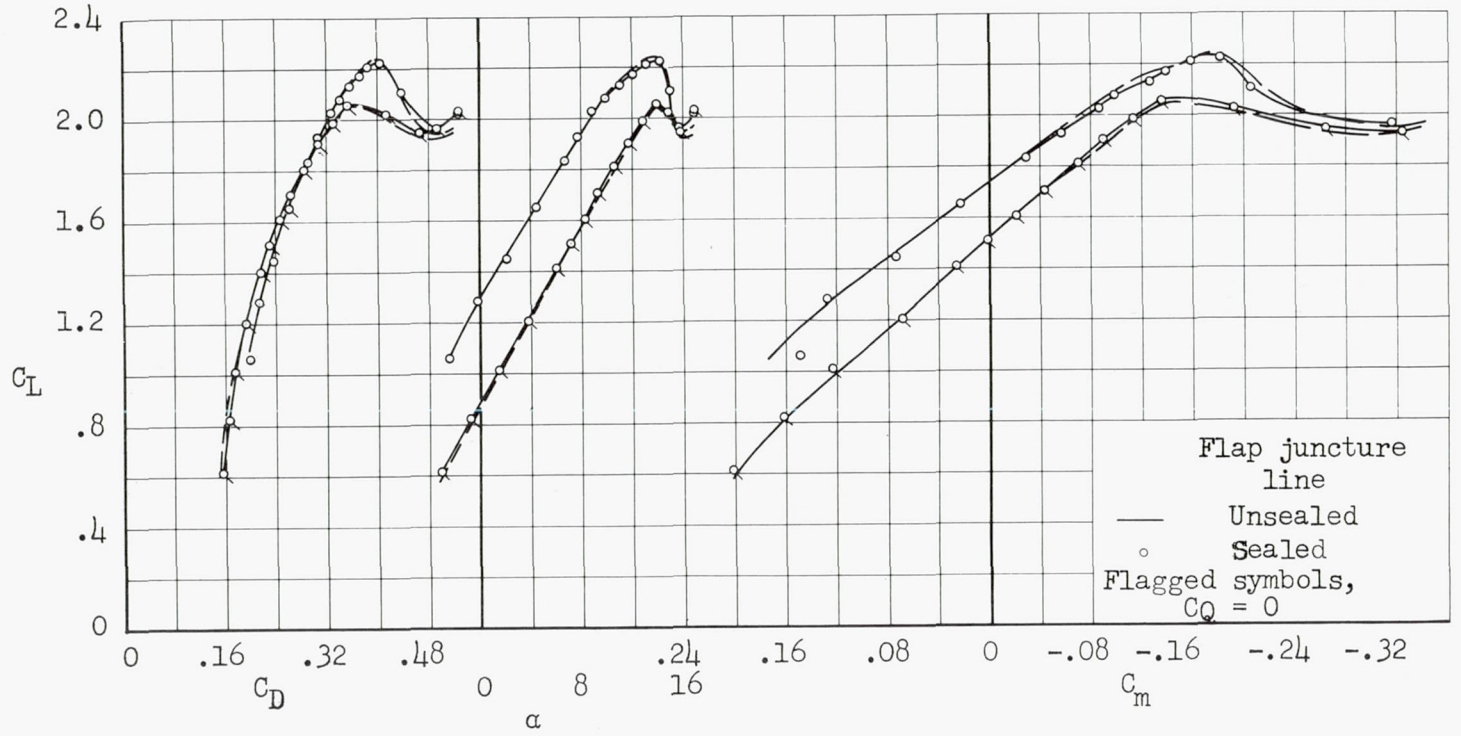

Figure 27.- Effect of sealing the flap juncture line on the aerodynamic characteristics of the complete airplane with plan form 2, slats M_3, glove 4i, and area-suction flaps deflected 55°; R = 8.2×10^6.

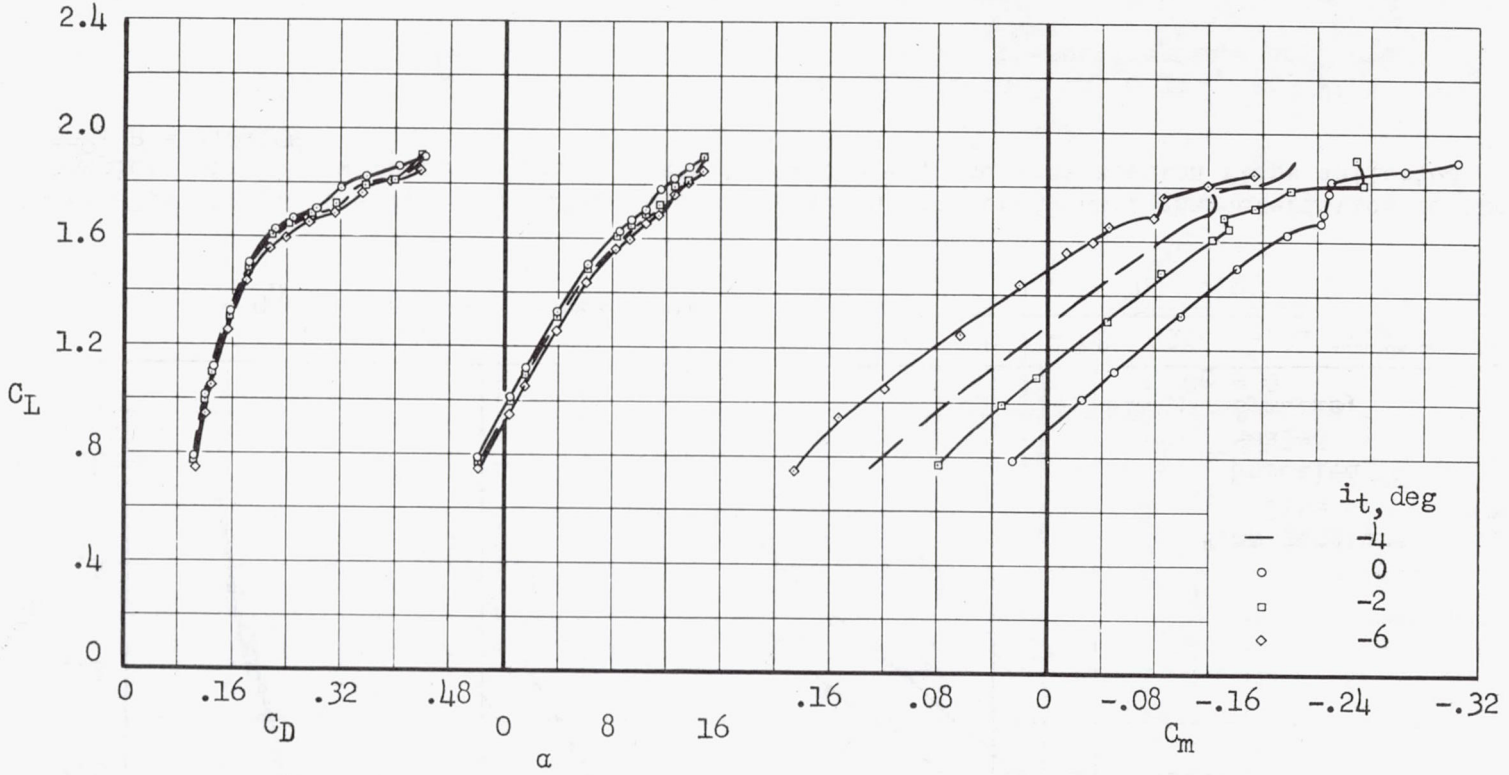

Figure 28.- Aerodynamic characteristics at several horizontal-tail incidences of the airplane with plan form 1, slats open, and slotted flaps deflected 36°; R = 10.5×10⁶.

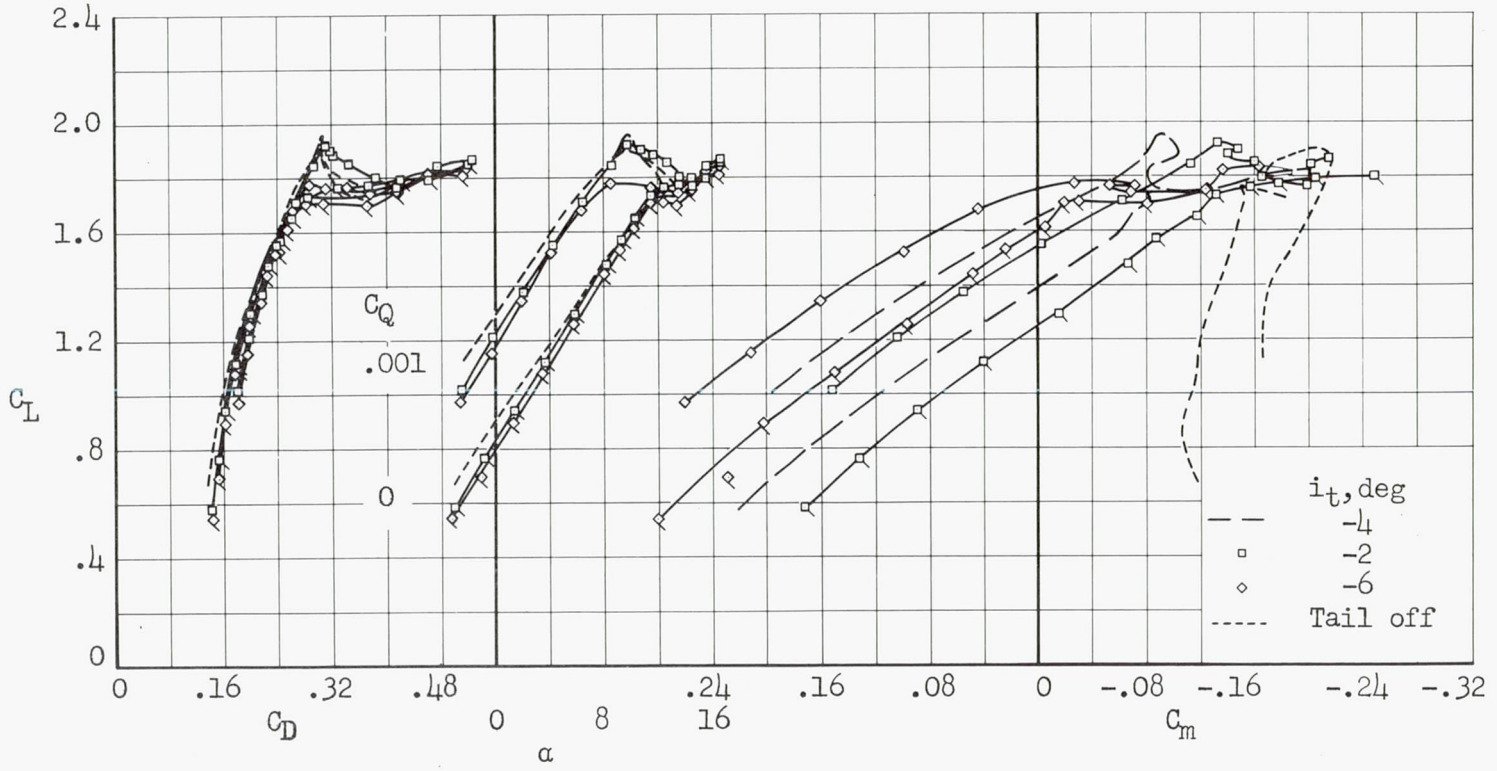

(a) Slats open, glove 2i.

Figure 29.- Aerodynamic characteristics at several horizontal-tail incidences, and with the horizontal tail off, of the airplane with plan form 1 and area-suction flaps deflected 55°; $R = 8.2 \times 10^6$.

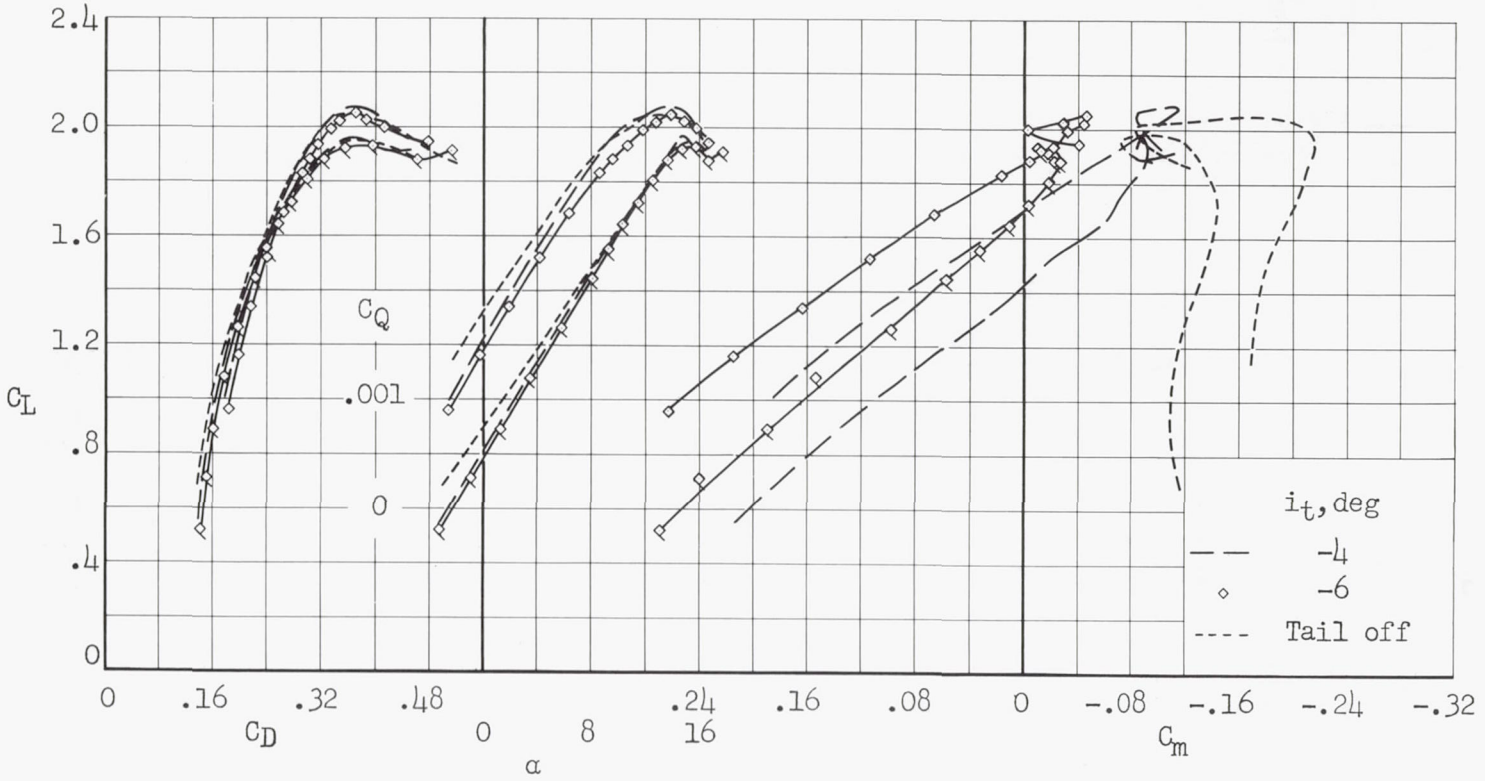

(b) Slats open, glove 4i.

Figure 29.- Concluded.

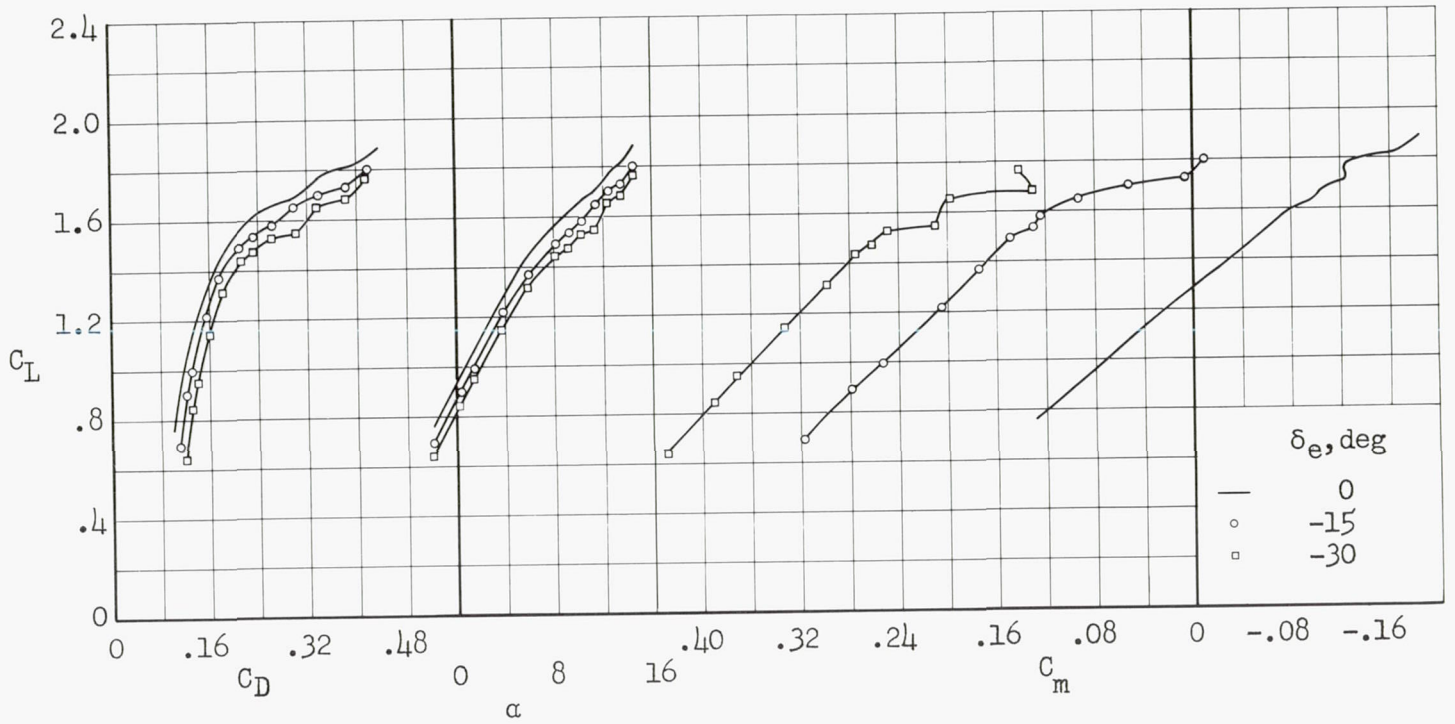

Figure 30.- Effect of elevator deflection on the aerodynamic characteristics of the airplane with plan form 1, slats open, and slotted flaps deflected 36°; R = 10.5×10^6.

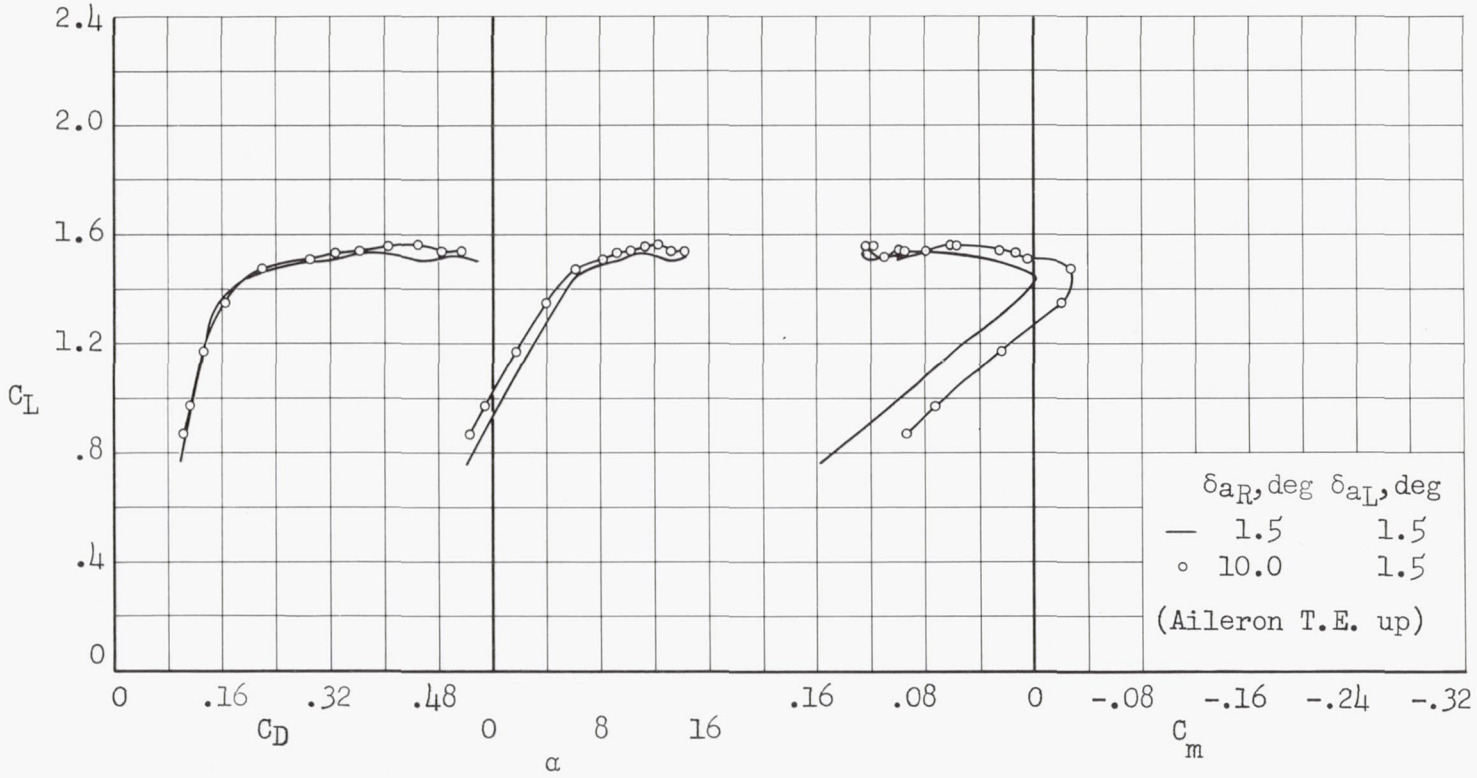

(a) C_D, α, and C_m vs. C_L

Figure 31.- Effect of aileron deflection on the aerodynamic characteristics of the complete airplane with plan form 1, slats closed, and slotted flaps deflected 36°; R = 8.2×10^6.

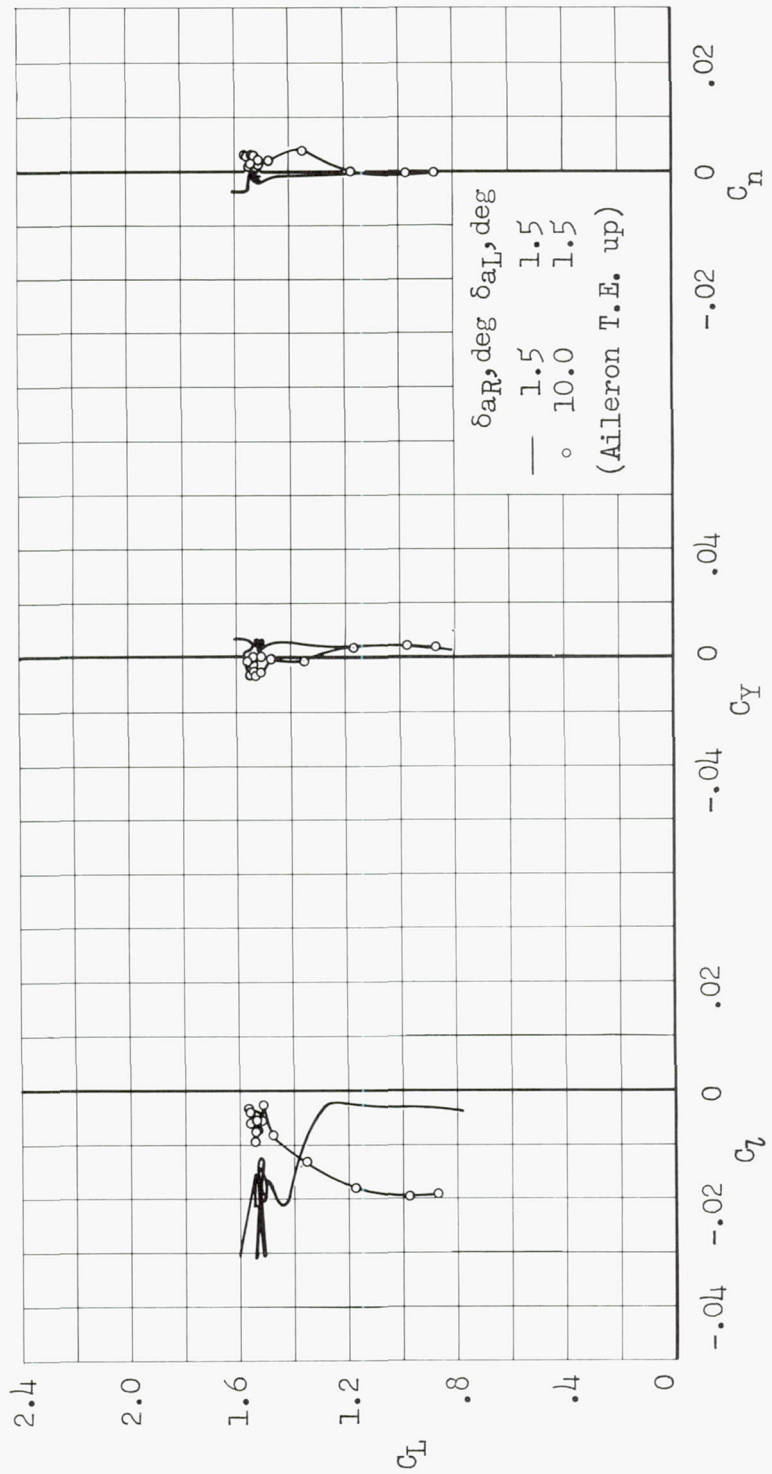

(b) C_l, C_Y, and C_n vs. C_L

Figure 31.- Concluded.

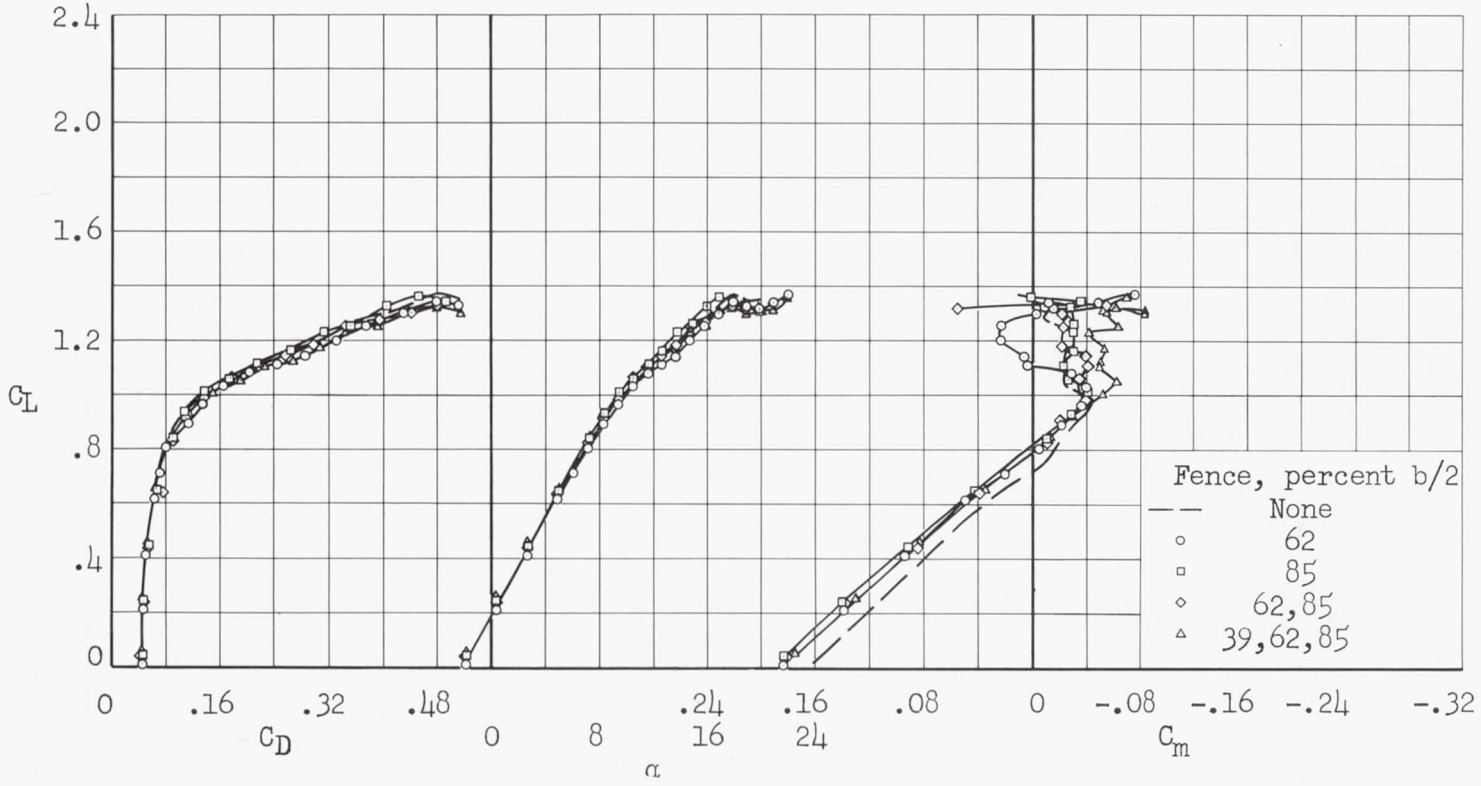

(a) $\delta_f = 0^\circ$

Figure 32.- Effect of full-chord fences on the aerodynamic characteristics of the complete airplane with plan form 1, slats closed, and slotted flaps; $R = 8.2 \times 10^6$.

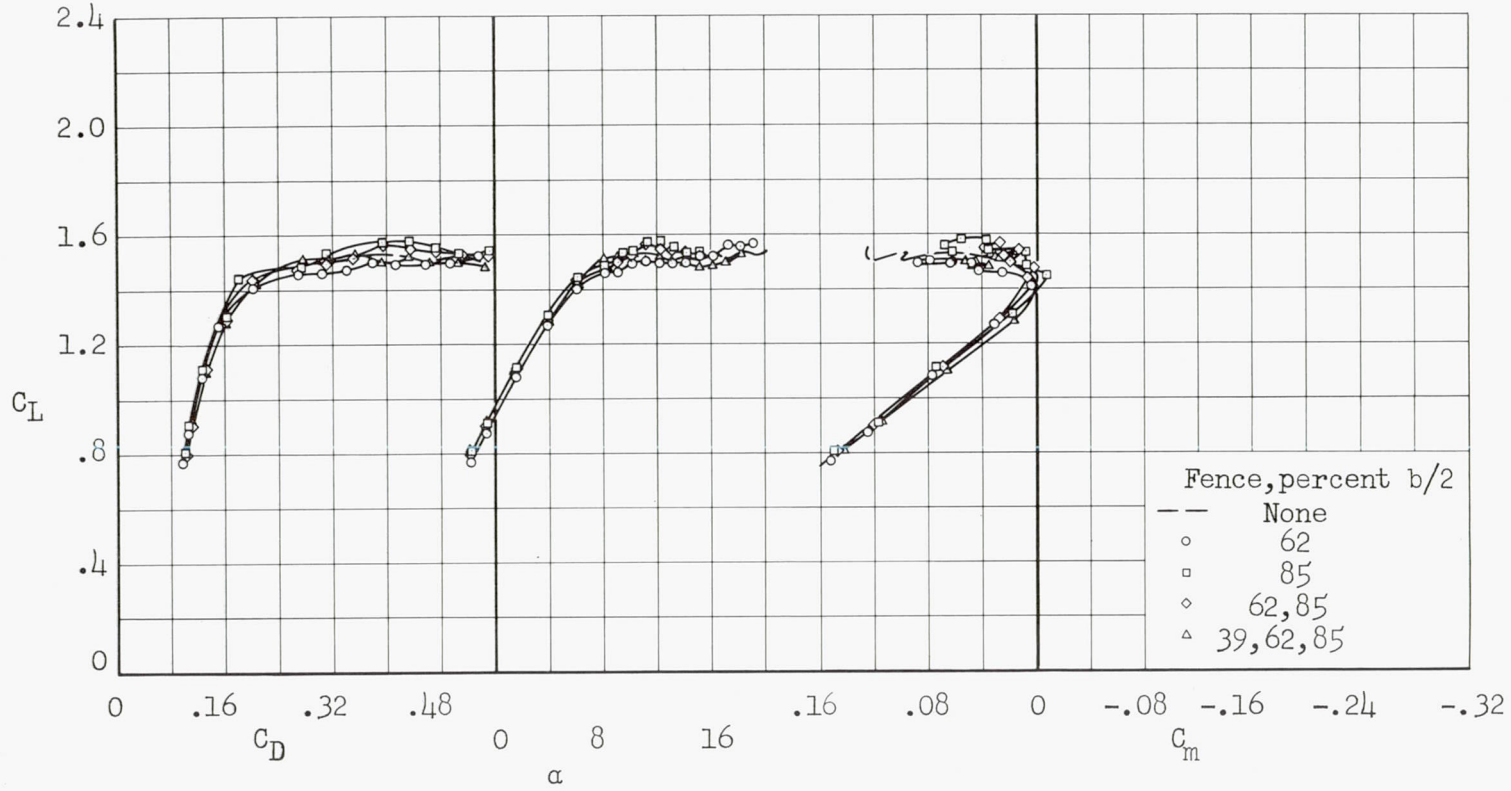

(b) $\delta_f = 36^\circ$

Figure 32.- Concluded.